2015

Copper in ultrapure water

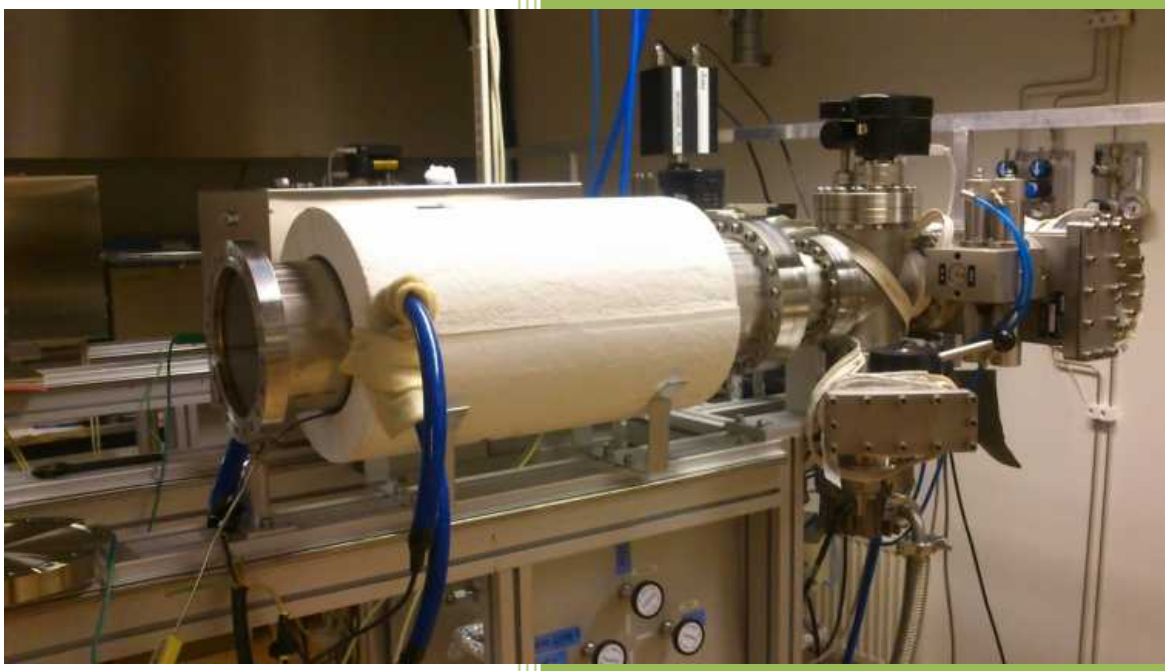

Mikael Ottosson, Mats Boman, Pedro Berastegui, Yvonne Andersson, Maria Hahlin, Marcus Korvela, Rolf Berger

Department of Chemistry –Ångström Laboratory

Contents

1. Introduction

1.1 Background

In a previous report (Boman et al. 2014), results were reported from long-term experiments (up to 6 months) concerning the possible corrosion of copper in ultrapure water, free from molecular oxygen. Claims that copper is not inert towards water but corrodes rather heavily, as indicated by the evolution of hydrogen gas, formed the background for the investigations (Hultqvist 1986, Szakálos et al. 2007, Hultqvist et al. 2009, 2011). In the current study, the pressure evolution of hydrogen gas was recorded in similar equipment as used by previous researchers (Further references in Boman et al. 2014), but the main focus was put elsewhere, namely on identifying oxidation products containing copper as a more conclusive indicator of copper corrosion. The search for such species entailed copper itself and its near environment within the closed system of the experiment. Thus, the copper, the water and the glass in contact with copper and glass were all thoroughly characterised by various sensitive analysis methods (See Table 1.1), both before and after experiments. The materials were of highest purity, and strict measures were taken as to avoid contamination during handling, including steps before chemical analysis.

Table 1.1. Acronyms and their encoding of the analysis methods having been used.

Analysis method	**Physical principles***	**Application (aggregation state)**
XPS	X-ray photoelectron spectroscopy	Element analysis (*s*)
AES	Auger electron spectroscopy	Element and phase analysis (*s*)
XRF	X-ray fluorescence spectroscopy	Element analysis (*s*)
LECO	Fusion analysis	Gas analysis (*s,l*)
QMS	Quadrupole mass spectrometry	Phase analysis (*g*)
ICP-MS	Inductively coupled plasma mass spectrometry	Element analysis (*l*)
ERDA	Elastic recoil detection analysis	Element analysis (*s*)

* For details concerning the various methods, see Boman et al. 2014.

As announced previously (Boman et al. 2014), further experiments were waiting for evaluation, in particular analyses of samples exposed to water for still longer times. Moreover, there were some issues concerning hydrogen loss or uptake with proper analysis which have now been addressed.

Another question that has arisen, as an effect of the deviation of our results in comparison with the original statements concerning copper corrosion in water, is whether the surface condition (dislocations, mechanical strain and macroscopic topography) might be a crucial factor influencing the reactivity. Therefore, some tests were made where the surface of the copper was scratched.

1.2 Structure of the presentation

The report consists of two parts, the main text and an appendix. The appendix presents some details of apparatus, calculations or analysis results.

The disposition of the main text is meant to primarily illustrate the progress of the work since the previous report: Section 1 (Introduction); Section 2 (Developments); Section 3 (Results and comments); Section 4 (Discussion and conclusions), References and Appendices.

2. Developments

2.1. Additions and alterations strategy

The equipment was thoroughly described in the previous report (Boman et al. 2014). The heart of the experiments lies in having pure copper in contact with water. The water is contained in a beaker made of glass with the highest hydrolytic resistance commercially available. The beaker rests in a vessel of stainless steel equipped with a lid where a membrane of palladium metal allows for the free passage of hydrogen through it. Such a vessel may stand freely in a glove box for a certain period while hydrogen escape through the palladium membrane, until the vessel is opened by dismantling the lid, and the contents are transported away for analysis. We have now data available for longer times than the 1, 3 and 6 months previously reported, extending the exposure time under the very same conditions as before.

As a complementary method to XPS concerning the surface analysis of copper, we also used a dedicated AES instrument with a scanning mode, using an electron beam. There are certain advantages with this approach: In the scanning mode (as in SEM) one can see where the electron beam will hit and the analysed area is definitely smaller than that probed by photons in an XPS instrument. Moreover, because only electrons are involved the surface sensitivity is enhanced. The reason for this approach was to find out whether the composition of a grain boundary was different from bulk, since contaminants have a tendency to accumulate between the grains. This instrument was not “in house” so the number of analyses was therefore limited.

A few of the vessels were used for monitoring the pressure, *i.e.* these were connected to a system with data logging facilities. On monitoring the hydrogen pressure, it had been found that the design of the fitting where the palladium membrane was clamped between the two compartments did not preclude that hydrogen gas also escaped from the system: Hydrogen was able to leave the palladium membrane through its edges. Therefore, this lateral leakage made a trustworthy estimation of the total hydrogen production difficult. Still, the attained pressure rise was more than expected from a direct chemical correspondence with the amount of observed oxidation products involving copper. Furthermore, as a complementary control of the hydrogen sources, measurements were performed to check the hydrogen content of the copper after the purification procedures previously described (Boman et al. 2014).

Thus, constructive measures were taken to ensure trustworthy readings and also to lower the hydrogen background in the pressure experiments. This strategy included changes of equipment and material properties. For establishing a certain connection between the observed hydrogen pressure and a corrosion process it must be possible to discern a net pressure increase compared to the background level. Since the observed amount of oxidized copper (predominantly expected as Cu_2O) was found to be very low (Boman et al. 2014), the corresponding reduction product (hydrogen gas) must also be very low. As a consequence, very harsh requirements were needed to bring down the hydrogen background pressure. Two main approaches were conceived, one aiming at decreasing the hydrogen background from the stainless steel and other parts involved, and one to completely ensure that hydrogen could not leave the system of interconnected compartments.

2.1.1 Modification of the vessels with new lids and pressure gauges

Two of the stainless steel vessels (SS 304L) that were meant for monitoring hydrogen pressure were machined (lathed) to an outer diameter of 70 mm so that the total volume of the steel was considerably reduced with the size of the inner void of the reaction chamber intact (See **Fig. 2-1**). Less volume made heat-treatment possible in a UHV furnace (**Fig. 2-2**) which was made for one of them, equipped into the setup called Main 3 A previous vessel that was not UHV-treated but treated in air (see below) was used in the Main 2 setup (See **Table 2-1**).

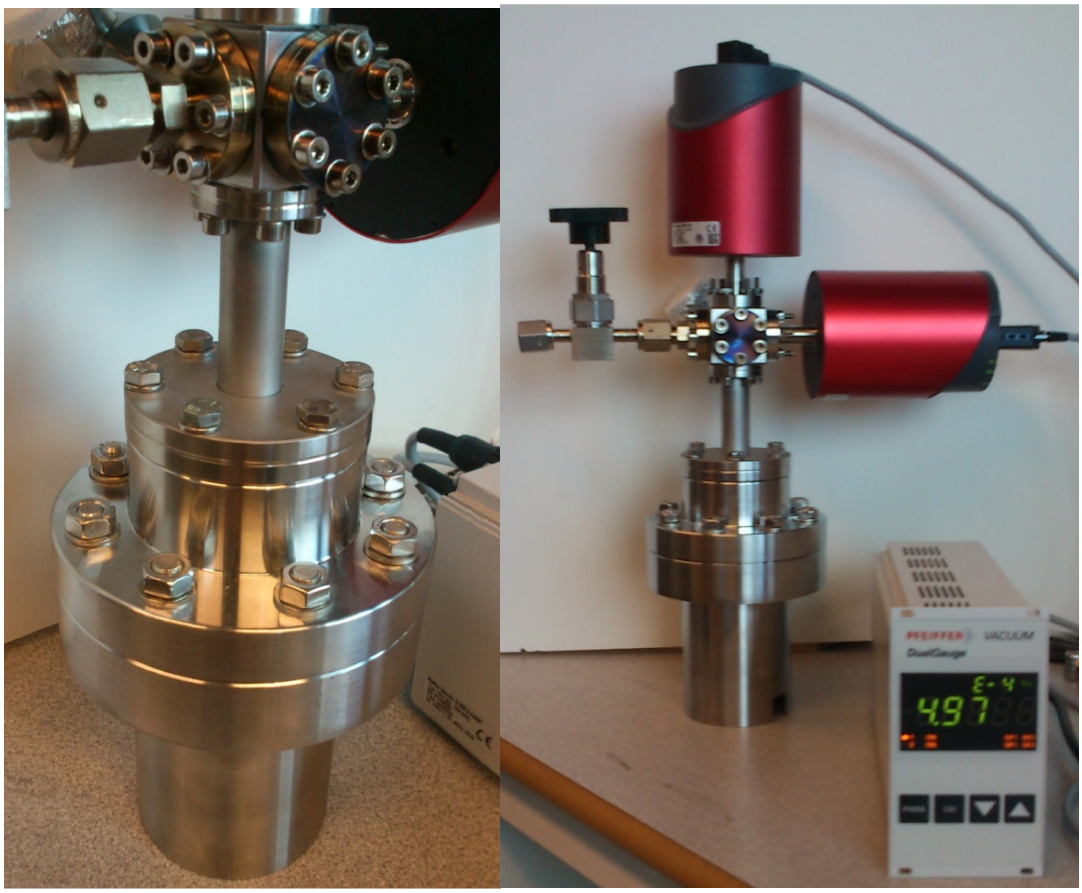

Fig. 2-1. *A new setup for pressure measurements (Main 3) equipped with a new lid including the Pd membrane (cf. Fig. 2-3). The diameter of the lower chamber has been reduced.*

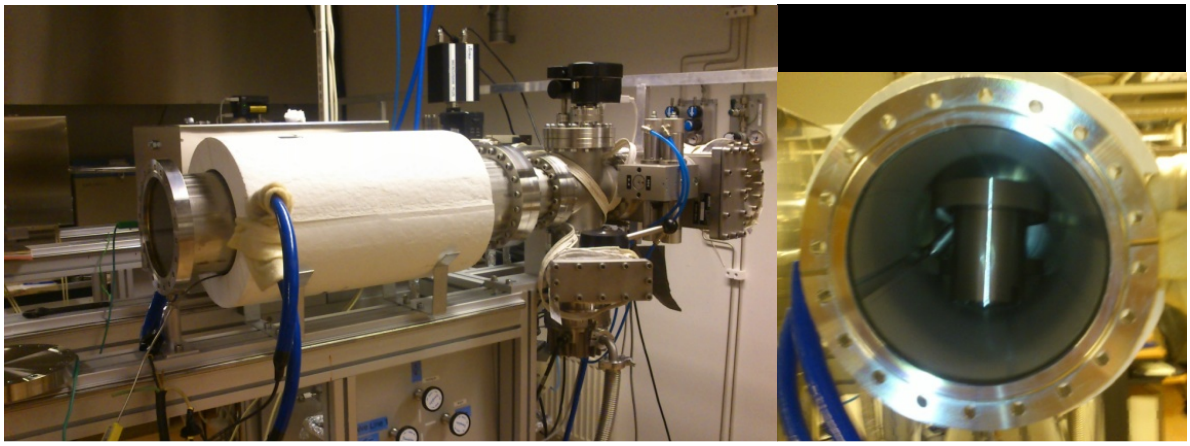

Fig. 2-2. *UHV furnace with the size-reduced stainless-steel vessel for Main 3 inside.*

Previously we noted (Boman et al. 2014) that hydrogen most probably seeped out laterally through the palladium membrane. The leaking rate was enhanced on increasing internal pressure, and ultimately a situation was reached where the hydrogen production rate and leaking rate were more or less equal. Consequently, another technical solution had to be found.

In the new design of the connection between the measuring and reaction chambers (*i.e.* the lid with its Pd membrane; see **Fig. 2-3** and details in **Appendix A**), no hydrogen at all can leave the system. In comparison with the former construction (in Main 1 and reference setups), the diameter of the membrane is now reduced with a factor of 2. Therefore, the increase rates of the pressure curves cannot be directly compared with those of Main 1. The new design was fitted onto the vessels of Main 2 and Main 3. Testing of outgassing was made without Pd foil after another baking out at 150°C for 5 days ("postbakeout"). This was followed by a blank test with Pd foil and loaded reaction chamber (but without copper).

New pressure gauges were connected to the Main 2 and Main 3 setups. Main 2 was equipped with one Pfeiffer CCR 374 (0-88 mTorr) and Main 3 with two, one for the 0-88 mTorr range and the other for 0-1.00 Torr **(Fig. 2-1).** The reason for the change of pressure gauges was to strongly reduce the outgassing rate from these parts, since they may emit hydrogen themselves at a considerable rate and cannot be baked out (See **Appendix A**). Comparisons between the new and old setups are shown in **Table 2-1**.

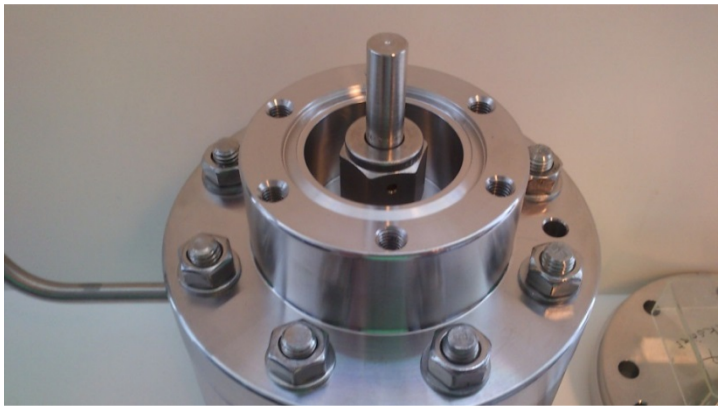

Fig.2-3.*The new lid, here with blind VCR ¼" connection together with the outer CF-38 seal.*

Table 2-1. *Comparisons between old and new setups*

Description*	**Main 1**	**Main 2**	**Main 3**	**Complement**
General	See Boman et al. 2014	New setup	New setup	New setup
Lower chamber	304L	304L	304L	304L
Upper chamber	304L	304L	304L	304L
Lid	304L	New: 316L	New: 316L	New: 304L
Outer diameter of chamber	114 mm	114 mm	70 mm (final wall thickness 3.5 mm)	114 mm
Diameter and weight of Pd membrane	20 mm 0.38 g	10 mm 0.10 g	10 mm 0.10 g	10 mm 0.10 g
Pressure gauges	MKS 627B	Pfeiffer CCR 374	Pfeiffer CCR 374	MKS 627B

*including stainless steel quality

2.1.2 Heat treatments of the setups

Two stainless-steel qualities have been used for the equipment, either 304L (upper and lower chamber) or 316L (lid). The L-sufficed qualities have lowered maximum carbon content compared to 304 and 316 with as a main effect better corrosion resistance vs. weld decay, *i.e.* especially developed for increased weldability. The European 316 qualities contain molybdenum, an alloy addition that in particular affects the tendency for pit corrosion in sea water (effects of chloride). For the application in this study, the choice between 304L and 316L is not germane in that respect (Jones 1992).

However, it is more relevant in the context of the present experimental situation to consider whether there is a pronounced difference in outgassing properties between 304L and 316L. A thorough study of the properties after proper heat treatments shows that there are no essential differences between them in that respect (Park et al. 2008). The authors also present a scheme how to reduce the outgassing by heat treatment in vacuum and air followed by postbakeout at a lower temperature.

The outgassing rate of hydrogen by the previous set-ups (Main 1 and old Main2) were typically $2\text{-}3 \cdot 10^{-11}$ torr·L/s·cm^2, yielding about $3 \cdot 10^{-5}$ moles/year as hydrogen background. This value is two orders of magnitude larger than the hydrogen evolution corresponding to the maximum copper corrosion rate of about $3 \cdot 10^{-7}$ moles/year, as estimated by Boman et al. (2014) from analyses of copper-containing species. In order to significantly discern hydrogen emanating from a copper corrosion process, the hydrogen background pressure encountered in the experiment had to be reduced by at least two orders of magnitude.

For UHV steels such as 304L and 316L, an outgassing rate of about $3 \cdot 10^{-11}$ torr·L/s·/cm^2 is normal for a bakeout at 150˚C for 50 h (O'Hanloon 2003). In order to reduce the outgassing significantly, temperatures of about 400 - 450˚C should be used (Park et al. 2008). This treatment will reduce the outgassing level down to the 10^{-13} torr·L/s·/cm^2 range.

As a vital comment to the heat treatments, one must stress that some parts were not bakeable at higher temperatures. Such limitations are considered in the summary of **Table 2-2**. As a consequence, each component was baked individually at appropriate temperature before the assembling of the setup. All CF and VCR components, except the UHV valve, were baked out at 400°C or 440°C.

Table 2-2. *Individual components and the maximum baking-out temperature*

Component	**Maximal temperature**
CF parts, lid and chamber	400-450˚C
UHV valve (copper seal)	400˚C, under vacuum
VCR-fitting	537˚C
Svagelock valve VCR	315˚C
Pfeiffer CCR 374 pressure gauge; MKS 627 B pressure gauge	50˚C

Two different methods (See Table 2-3 for details) for bakeout were tested:

- **Main 2**. Baking in air to oxidize the surface of the stainless steel; the high temperature is expected to reduce the hydrogen content. The oxide surface layer is also expected to increase in thickness which should reduce the outgassing from the bulk of the steel (Bills 1969). This method did not give a low outgassing rate (2 10^{-5} mole/year; see appendix A) and an additional annealing was therefore performed at 300˚C in UHV.

- **Main 3.** In this second approach a large UHV furnace was used for heat-treating the individual components under UHV conditions. A low hydrogen pressure is expected to yield a faster outgassing rate of the hydrogen (Park et al. 2008).

The chosen schemes of the heat treatments of the vessels are shown in **Table 2-3**. As summarized there, the treatments are fundamentally different (heating in partly in air or not) for the setups used for Main 2 and Main 3. Thus, the outgassing behaviour may be different between the two, although the stainless-steel qualities and internal volumes are the very same.

Table 2-3. *Heat treatment schemes for the stainless-steel compartments.*

Vessel for Main 2:		**Vessel for Main 3:**	
Temperature	**Time**	**Temperature**	**Time**
150°C [c]	Overnight	150°C [c]	Overnight
400°C [a]	96 h	300° - 400°C [c]	5 days
400°C [b]	2 h	440°C [c]	3 weeks
300°C [c]	240 h		

[a] argon; [b] air; [c] UHV, typically 10^{-9} Torr.

2.1.3 Complementary setup outside glove box

A special setup was designed for testing various background and pressure relaxation effects. It was not thoroughly baked out (only kept at 150°C), being an old setup equipped with another lid made of 304L stainless steel (See Table 2-1) to fit the new improved membrane connection. In contrast to the live experiments in the glove box, this setup was modified to allow pressure measurement also in the lower chamber (corresponding to the reaction chamber with copper and water).

Two MKS pressure gauges were attached to the upper chamber for up to 0.05 and 1.00 Torr, respectively. Another gauge (1.000 Torr) measured the pressure of the lower chamber, attached through a ¼” tube welded to it.

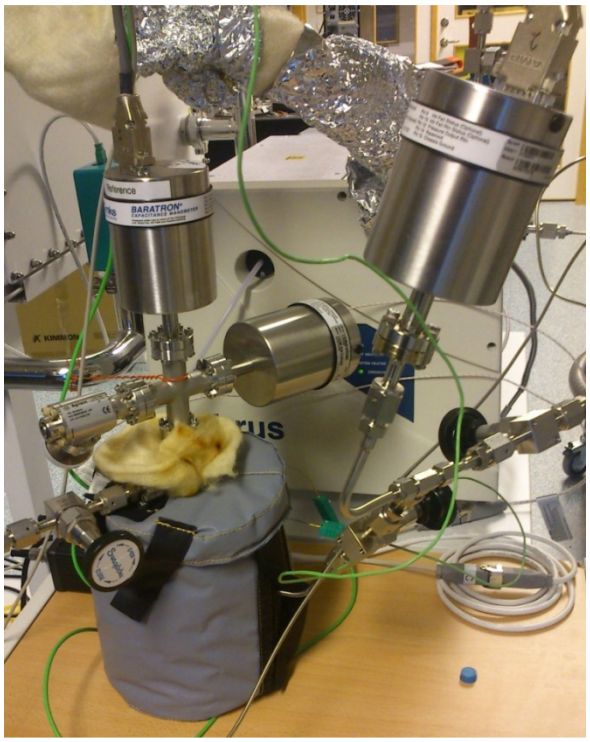

Fig. 2-4. *Complementary setup for pressure measurements outside the glove box.*

This setup does not have direct bearing on the copper corrosion experiments but focuses on issues concerning the exchange between reaction and measuring chamber. Furthermore, the background has not been decreased by extensive heat treatment but only at 150°C. Therefore, the hydrogen pressure regime in this setup is certainly higher than in those used in the corrosion experiments. Still, essential features of the exchange could be investigated and shed light also on the situation occurring for the setups containing copper in corrosion experiments. Since the setup deviates in many respects and all effects cannot be conveyed directly to the corrosion experiments, data concerning this setup are found in **Appendix C**, rather than here.

2.2 Determination of hydrogen content

It has not been established whether the hydrogen content of copper itself might influence the corrosion properties, *e.g.* whether a high content of dissolved hydrogen might reduce the reactivity of the copper. This suggestion has emerged as a tentative explanation of the low corrosion rates observed by Boman et al. (2014), connected to the practised purification of copper containing a step of heat treatment in hydrogen gas. No support of that idea has been found in the literature. In Boman et al. (2014) the problem of establishing the concentration of dissolved hydrogen had been addressed by using two methods, ERDA and fusion analysis.

Although seemingly promising because very low contents should be detectable by ERDA, the fact that the equipment was not tuned to solving this kind of problem led to difficulties in interpretation. After the publication of the report by Boman et al. (2014), it has become clear that the technique often tends to overestimate the contents of hydrogen (and, as a further drawback, it is not able to distinguish between free or chemically bound hydrogen). In Boman et al. (2014, Section 5.2.3 and Appendix D2), an ERDA analysis was reported and its level of significance was also discussed. No direct measurement could be made, leading to

analyses resting on modelling only. Therefore, it is recognised in retrospect that ERDA was not a good method to be applied to the problem of so low hydrogen contents for attaining high accuracy. As a consequence, this method was discarded for further analyses.

For hydrogen analysis, the melting analysis method (LECO) was used by the supplier (Alfa Aesar) as shown for only one of the batches of copper that were used in our experiments. However, it seems to be common practice by this technique to mechanically remove the surface layer of specimens before the metal is melted during a rather short heat run. This procedure to get rid of oxide (that would influence the apparent hydrogen content) cannot be easily applied to thin sheets, so we suspect that the analysis results quoted in the supplier's analysis certificate have in fact been performed on pieces of copper taken out of a batch before processing the copper into thin sheets. If that is the case, the value presented in the analysis certificate is not necessarily applicable for the processed copper – but the supplier has not responded to our specific questions on this issue. Moreover, the values presented in Boman et al. (2014, Section 5.2.4 and Appendix D1) were obtained on too little material (too low mass) or without repetition which precluded satisfactory statistics.

This kind of measurements was afterwards applied again under more controlled conditions in coordination with another analysing company (Degerfors Laboratorium AB), where we were also able to influence the measuring strategy since our sample deviated from what was fit for their routine procedures. Samples are – if need be – surface-polished by a diamond cloth, and transferred to the instrument, a Leco ONH-836 Elemental Analyser. The samples then get melted in a graphite crucible under He atmosphere. The hydrogen that is released reacts on a copper oxide catalytic converter to form water. The water content is determined by IR spectroscopy with calibration towards standard materials. As encountered before, problems with small sample sizes prevailed (See **Appendix E** for a discussion).

Considering the issue of hydrogen content of copper in connection with sample treatment, samples were also investigated in another way. In the purification process of copper described in Boman et al. (2014, Section 2.2.1 and Appendix C1- C3), the last two steps involve the reduction of superficial oxides (from electropolishing) by H_2 at 300°C followed by annealing in vacuum at 400°C. During the latter step, the outgassing of hydrogen was then monitored by mass spectrometry. The same methods were now also applied to various copper samples in order to study the outgassing, but using a broader temperature range to yield more information on the copper quality and on the processes involved.

3. Experimental results with comments

3.1 Overview

In order to make the results easier to follow, we first present an overview of the various experimental "stations" that have been operating, aiming at a complete picture of the situation. For clarity, we therefore also include measurements on samples already reported on. Appropriate data are all collected in **Table 3-1**.

Table 3-1. *The various experiments and their evaluation*

Experiment station	**Type of experiment**	**Chemical analysis techniques***
Free-standing, 0 months[a]	Oxidation products	XPS/AES, ICP-MS, XRF, LECO[b]
Free-standing, 3 months[a]	Ditto	XPS/AES, ICP-MS, XRF, LECO
Free-standing, 6 months[a]	Ditto	XPS/AES, ICP-MS, XRF, LECO
Free-standing, 15 months	Ditto	XPS/AES, ICP-MS, XRF, LECO
Free-standing, 29 months	Ditto	XPS/AES, ICP-MS, XRF, LECO
Main 1 (from beginning) [b]	Pressure measurement	*Pending*
Main 2 (new equipment)	Ditto	XPS/AES, ICP-MS
Main 3 (new equipment)	Ditto	*Pending*
Complementary setup	Ditto	*Not applicable*

* For the acronyms, see Table 1-1; [a]Description and results in Boman et al. (2014); [b]New data added

In Boman et al. (2014), data were collected and the results were reported for the exposure times 1, 3 and 6 months concerning the long-term semi-open vessels, *i.e.* those that were not connected for pressure measurement but allowed passage of hydrogen out into the glove box. Now those that were run for 15 and 29 months have been investigated, and the trend may be followed in an extended time frame (in fact there is still an unopened vessel). The analyses apply to copper and its near environment (water), as well as the glass in contact with that water. The analysis methods were described in Boman et al. (2014) and are discussed here only where considered appropriate.

The modified Main 2 and Main 3 setups were assembled for pressure measurements. As an interesting addition to previous procedures, two samples of purified copper (99.9999%, surface treated) were now also scratched, considering that surface morphology and mechanical strain might influence the reactivity towards water. The scratching of the copper foils was done manually on both sides inside a glove box with nitrogen atmosphere. However, the manual scratching implies inadequate reproducibility compared to the case with an automated technique. In order to rule out the possibility of galvanic cell formation, two materials of different electronic conductivity were used for the surface treatment, SiC paper (Struers, 320 grit size – 40 μm) and diamond powder (Diamantprofil AB, type MB-1-UM, 30 mesh). In the latter case, two copper foils were rubbed against each other with a small amount of diamond powder in between. No signs of diamond particles on the surface could be found from examining under a microscope.

That scratched samples may behave differently gets some support by the observation (Johansson et al. 2015) that SiC-scratched copper may evolve hydrogen during a limited time (up to a few days) after immersion. In order to not confuse this possibly temporary process with longer-term hydrogen evolution, the diamond-scratched copper foils were subsequently

kept in oxygen-free ultrapure water for six days prior to loading them into the reaction chamber. This measure was not taken for those scratched by SiC.

After loading, the setups were evacuated (only upper chambers possible) for a couple of days before starting to monitor the pressure. The contents of both setups were subject to complementary chemical analyses (Table 3-1).

Both setups used the revised steel containers equipped with the new lid construction for the palladium foil, so as to not to allow any hydrogen to leave the system. The new equipment had to be thoroughly investigated with regard to the hydrogen background levels since the outgassing rate must be different from before by all the changes, not the least through the extensive heat treatments and change of pressure gauges.

The complementary "bench setup" was used for testing various ideas concerning effects that might be relevant for the interpretation of the experimental outcomes of the pressure measurements of Main 2 and Main 3, with the focus on the palladium foil interface. These experiments (**Appendix C**) never included copper or water.

The "old" Main 1 setup has been running since the start of the experiments (Boman et al. 2014) and not undergone any instrumental changes. Pressure measurements have been made continuously over all this time. Data for this setup are given in **Appendix F**, where recent experiments concerning behaviour on temperature change are included.

3.2 Pressure measurements

3.2.1 General remarks

For establishing whether there is any significant hydrogen production from copper due to corrosion in the water, the influence of the background has to be taken care of through trustworthy measurements of the pressure. It is then crucial that all important aspects of the experimental situation are taken into serious consideration. Because of the low production rate of hydrogen from the anticipated limited corrosion process, the total hydrogen emission present in the equipment has to be evaluated properly. The geometry of the setup is principally a division into two parts, one where the corrosion reaction may take place (the reaction chamber) and one where the pressure is measured. The interface in between the two compartments is the palladium membrane through which only hydrogen can pass. In view of this, one cannot neglect the influences of the Pd metal in order to correctly interpret the outcome of the pressure measurements.

The difference in experimental outcome of the equipment as regards hydrogen pressure measured is demonstrated in **Fig. 3-1**. The two measurements were performed with the Main 3 setup. It is unequivocally illustrated that the pressure readings, that are supposed to yield the hydrogen gas production rate, cannot be trusted from the assembly that encompasses the Pd membrane without corrections for its effects. (The pressure data presented in Fig. 3-1 were corrected only for difference in gas volume between the two cases. The measurement without Pd was made with an empty reaction chamber, and that with Pd also included the water-filled beaker.)

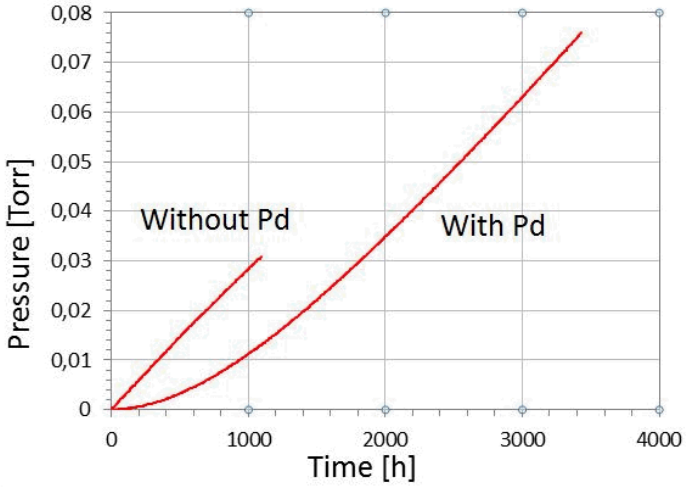

Fig. 3-1. *Pressure rise in a system with or without the Pd membrane between the two compartments.*

Hydrogen is the only gas that may pass the palladium membrane. What happens at the metal surface is a homolytic dissociation of the H_2 molecules into separate hydrogen atoms. These are small enough to diffuse into the metal crystal structure to form a solid solution. The driving force for any diffusion process is a difference in chemical potential, in most cases as a result of different concentrations. The dissolved hydrogen atoms thus tend to distribute themselves over the available voids in the palladium crystal structure. If there is a difference in pressure between the two sides of the membrane a steady state situation is eventually reached for the flow through it. With the present arrangement there may be different production rates for the two compartments, so the final situation reflects that fact. Before the steady state is reached, there are temperature and concentration dependent mechanisms that occur simultaneously and in succession (Ward and Dao 1999, Caravella et al. 2013). The final solubility of hydrogen within the membrane, valid in the single-phase regime found for low hydrogen contents according to Flanagan et al. (1976), is expressed by Sieverts' law:

$$X = K_s\sqrt{P}$$

Here, the K_s factor depends on the species that are involved and on temperature.

To compensate for the fact that the membrane takes active part in the hydrogen distribution, a simple model was used (See **Appendix B).** The model illustrates that hydrogen is to be found in the form of H_2 gas and within the membrane, the molar amounts being summed, but it fails to describe the situation properly at low pressures, with the effect that the hydrogen production rates get underestimated. A basic assumption behind this model is that equilibrium is pertained between the two chambers and the Pd membrane. Tests concerning this aspect were performed by the complementary equipment (**Appendix C**), the results of which indicate relatively long times for equilibrium to establish (but the pressures are different from those of Main 2 and Main 3).

$$P_{WoPd}=P_m + K_{exp}\sqrt{P_m}$$

P_m = The measured pressure
P_{WoPd}= The pressure without Pd
K_{exp} = Experimental constant, including K_s and volume factor

In order to make the results and the interpretation of the pressure experiments easier to follow, the experimental schemes are presented in connection to the illustrations of the graphs, rather than giving them in Section 2. All measurements (at 50°C) were started with measurement of the background before loading with respective copper sample.

The outgassing background was measured by two methods:

1. Vacuum outgassing, by measuring the increase in total pressure vs. time (without the palladium membrane). This was done after baking the setup (for about 5 days).

2. Background under experimental conditions, *i.e.* the pressure increase in the upper chamber with the Pd membrane mounted and water/sample holder in the reaction chamber. This was performed after loading the chamber with deaerated water inside the glove box.

The outcome according to the first method (blank) applied to Main 2 and Main 3, respectively, is illustrated in **Fig. 3-2** with numerical data for the outgassing rate in **Table 3-2.** The volumes are the same, so the difference must depend on the respective treatment of the stainless steel (see **Table 2-3**) and the temperature. The pressure rise due to hydrogen evolution from the container materials and measuring devices is essentially linear with time.

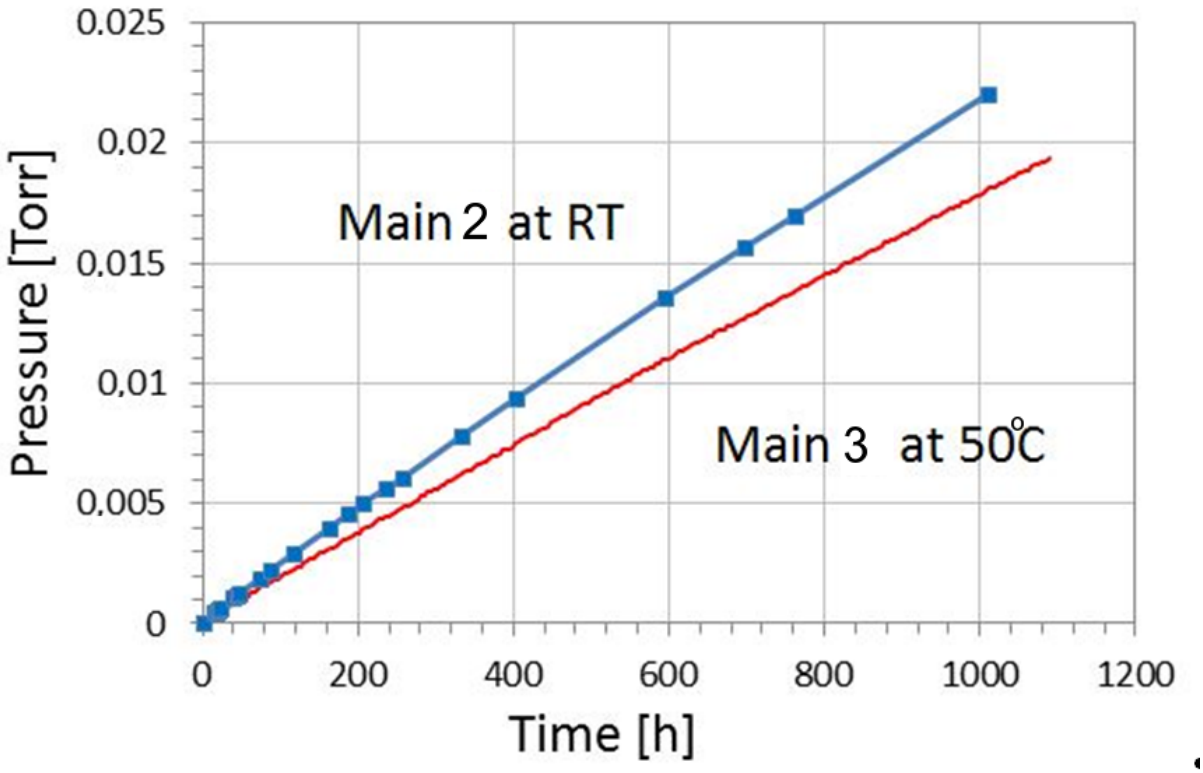

***Fig. 3-2**. Background measurements in Main 2 and Main 3 (at different temperatures; RT= room temperature, 25°C).*

Table 3-2. *Outgassing rates for the empty* setups (No Pd foil).*

System	Outgassing mol/year	Temperature
Main 2	$3.4\ 10^{-6}$	25°C
Main 3	$2.5\ 10^{-6}$	50˚C
Main 1*	$2\text{-}3\ 10^{-5}$	50˚C

*For comparison, data are included from Boman et al. (2014), however, for a loaded system including Pd-foil. The values are only estimations from the maximum pressure increase.

For Main 2 the background outgassing rate (See **Appendix B**) was determined from pressure measurement at room temperature (*cf.* Fig. 3-2) directly after baking at 300°C (*cf.* Table 2-3). Main 3 was assembled, and the upper chamber was baked out at 150-200°C for a few days before the measurement series.

Loading:
After introducing the Pd membrane (see further 3.2.2), Main2 was used for two series of measurements with copper residing in sample holders in water:

- SiC-scratched copper
- unscratched copper

Both samples were of 99.9999% purity and first polished and purified as described in Boman et al. (2014, section 2.2 and Appendix C).

After background tests (see further 3.2.3), Main 3 was similarly loaded with diamond-scratched copper of identical quality.

3.2.2 Main 2

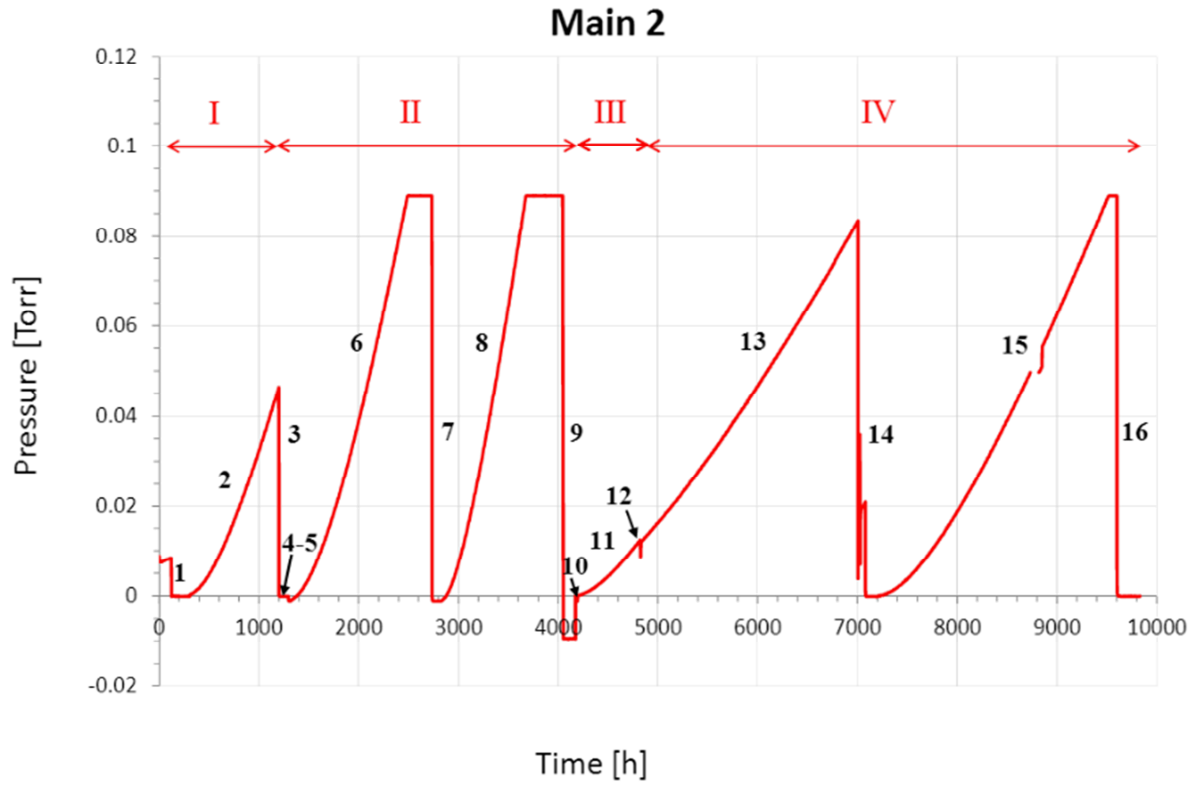

Fig. 3-3. *Results of the pressure measurements for Main 2. The numbering alludes to the measuring scheme given in text. The cut-off at 0.088 Torr is an artifact due to the limitation of the pressure gauge. The imperfection at about 8800 hrs is due to a flaw in the common logging system.*

The background was first measured without Pd membrane and water (See **Fig. 3-2** and **Appendix B**). The measurements (with Pd membrane) followed the scheme below, where four distinct regimes (I-IV) are discerned (*cf.* **Fig.3-3**):

I. 1. Evacuation.
2. Background measurements with water and sample holder
3. Evacuation

II. 4. Adding of SiC-scratched copper foils
5. Evacuation (roughly three days)
6. Pressure increase
7. Evacuation (the maximum of 88 mTorr being reached)
8. Pressure increase
9. Evacuation (the maximum of 88 mTorr being reached)

III. 10. Background measurements without copper samples
11. Pressure increase

IV. 12. Loading of unscratched copper foils (without evacuation)
13. Pressure increase
14. Evacuation (just before the pressure limit)
15. Pressure increase
16. Evacuation (pressure limit just reached); experiment stopped

The various curves of **Fig. 3-3** need to be commented and analysed. Please note that the SiC-scratched copper samples were measured twice (curves 6 and 8) with evacuation in between. Likewise, the background was measured twice, before (curve 2) and after (curve 10) the live samples. What is directly obvious from the results is the behaviour of pressure rise immediately after evacuation. The pressure increase is strongly deviating from a linear relationship with time which is interpreted as an effect of hydrogen uptake in the Pd membrane (cf. **Fig. 3-1**). This effect influences the accuracy of the pressure increase and is especially cumbersome for determining the net hydrogen evolution from copper. In order to obtain a more correct background, the application of modelling seems proper. Attempts in this respect are described in **Appendix B** and were used for estimations of the hydrogen outgassing rates, as illustrated in **Fig. 3-4** that is divided into the same regimes as Fig. 3-3 since they are related.

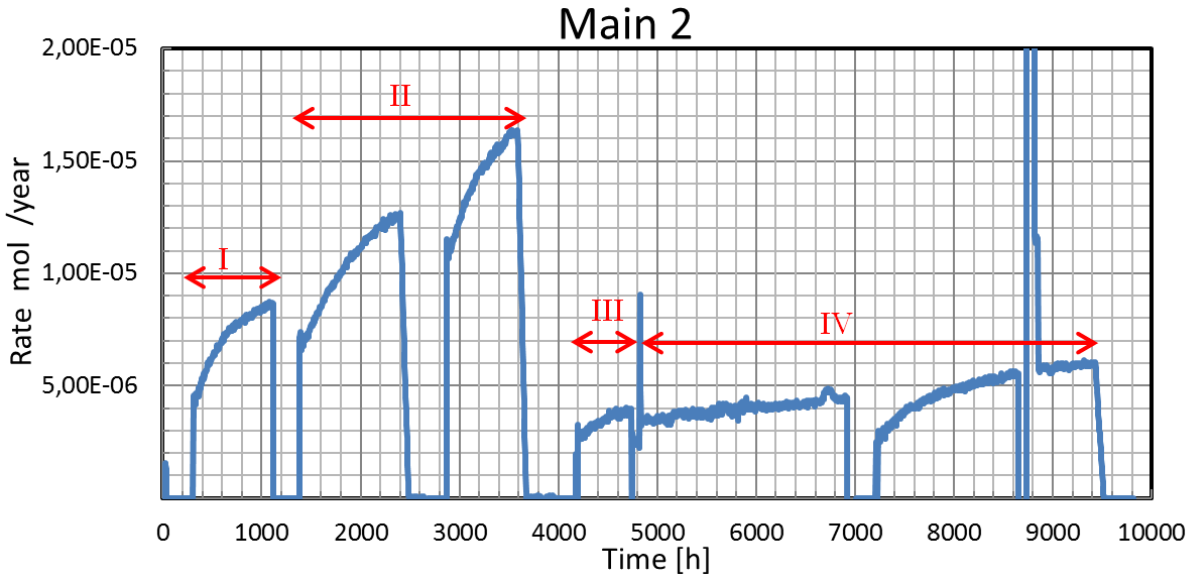

Fig. 3-4. *Plot of the same data as in Fig. 3-3 in the form of estimated hydrogen production rates. The irregularity in regime IV at about 8800 h is due to to a flaw in the common logging system.*

The background rates. The first background (curve 2 in regime I) starts at about 4 µmoles per year and increases with time to about 8 µmol/year after 800 hours (at 1100 h in Fig. 3-4). These values are considerably higher than obtained for the empty setup (3.4 µmol/year in Table 3-2). The second background (curve 11 in regime III) was measured after finishing the measurements on SiC-scratched copper (regime II) and is considerably lower. After a slight increase it levels out at about 4 µmol/year. That value is in better agreement with that obtained for the empty system.

The rates are not expected to depend very much on time. The observed behaviour is an indication of an unstable system, all the more since the rates also increase in regime II (see below). The origin of the increase is obscure and its solution lies outside the scope of this report. The curves of Fig. 3-3 looked rather normal (illustrating mainly the effect of the Pd membrane) and were not alarming, since they did not convey the strange behaviour of the system. It is noteworthy that the Main 3 system (**Appendix B 3**) does not show any similar instability; one difference is that it has undergone a different heat treatment (Table 2-3).

System with SiC-scratched copper. Like in the first background measurement, the rates observed for curve 6 and 8 (regime II) show an increase with time except when the process is interrupted. Curve 6 starts with about 7 μmol/year and ends with 13 μmol/year after 1000 hours (at 3600 h at the time scale) where the upper chamber was pumped out because the limit of the pressure gauge had been reached (See Fig. 3-3). The monitoring of curve 8 (same regime) commenced after 200 hours of pumping, yielding values of 11 - 16 μmol/year during 800 hours. Again the 88 mTorr limit was exceeded and the upper chamber was pumped out, ending the measurement session of regime II.

Here also, the rate seems to increase during the experiment that had to be divided within regime II due to the limited pressure range of the gauge. Whether the pressure rate would have levelled out after a long time is impossible to tell. The rates are definitely higher than that measured for the background. This indicates an enhanced hydrogen production but we cannot exclude artefacts. Because of the unexpected behaviour of the rate curves it is not possible to deduce any reliable rates from the present data. Further investigations are needed to understand the hydrogen evolution from SiC scratched copper. Again, we may allude to the findings by Johansson et al. (2015) from a similarly prepared sample that short-term effects may be at play.

A QMS analysis showed about 97 % hydrogen in the gas phase, an indication that the pressure increase is not due to a leak in the system. Otherwise, an enhanced nitrogen content would have been evident. The pressure increase must originate from hydrogen production within the system.

System with unscratched copper. The new sample was inserted (between III and IV) without pumping the upper chamber. A small pressure decrease was observed after the loading. The rate starts (curve 13) at about 3.5 μmol/year and increases up to 4.3 μmol/year during 2000 hours. Just before the pressure limit was to be attained, the upper chamber was pumped out. The series continued (curve 15) with the rate increasing from 3 μmol/year to 6 μmol/year during 2400 hours and was stopped at 9500 h on the time scale.

In this case, the rate evolution is less steep but it is, due to the limitations in modelling, not reliable to evaluate a net rate by subtracting background values. Further background measurements are needed (experiment is in fact ongoing). However, considering the values obtained, any hydrogen production with copper corrosion as its source must be very small (< 2 μmol/year).

3.2.3 Main 3

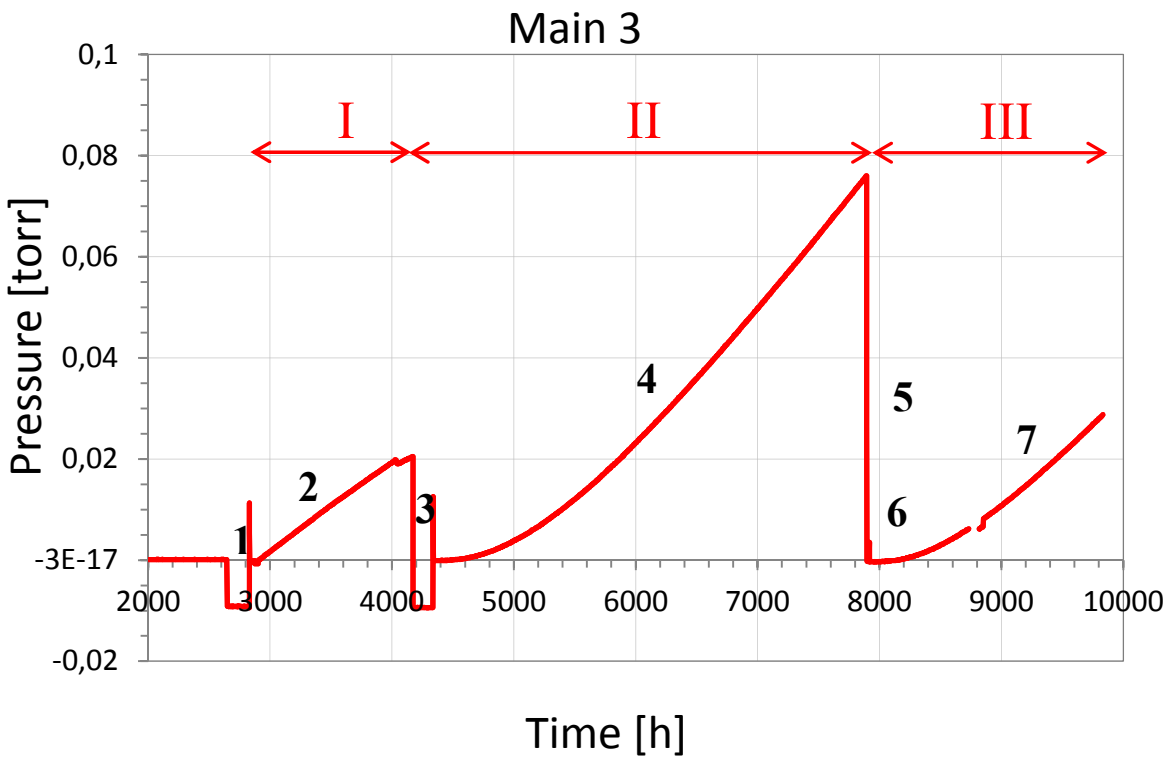

Fig. 3-5. *Results of the pressure measurements for Main 3. The jump in the pressure curve corresponds to the calibration of the pressure meters during evacuation. The imperfection at about 8800 hrs is a flaw in the common logging system.*

The handling deviated little from that of Main 2, using the same temperature and copper quality. However, in this case the scratching of the purified copper was made by diamond powder instead of by silicon carbide paper. After keeping them in water for six days, the foils were loaded into the lower chamber (in another batch of water). After pumping for about three days, the valve was closed and the pressure increase was monitored.

A similar measuring scheme for the pressure monitoring was followed as for Main 2, only that the background was measured twice before the introduction of copper. Three distinct regimes (I-III) are discerned (*cf.* **Fig. 3-5**):

I.	1. Evacuation.
	2. Background measurements without water and Pd foil (*cf.* **Fig. 3-2**)
	3. Evacuation
II.	4. Background measurements with water and Pd foil
	5. Evacuation
III.	6. Loading of diamond scratched copper foils + water
	7. Pressure increase

Background rates (I and II).
Background I (curve 2) does not contain any influence from the membrane. By direct measurement of the pressure increase, the outgassing background was determined from the slope of the pressure increase to 2.6 μmol /year (**Appendix B**).

Background II (curve 4) had to be calculated because of the deviation from linearity, an effect of the hydrogen uptake from the Pd membrane. The modelling (as for Main 2, omitting the low-pressure part) gave 3.5 μmol/year (**Appendix B 3**).

The diamond-scratched copper foils (III)

N.B. The experiment is still running (February 2015). The pressure increase (curve 7 of Fig. 3-5) is very similar to the background (curve 4). This is illustrated by the overlap of **Fig. 3-6**, being thereby an indication of a very low hydrogen production from the copper. An analysis is extremely demanding when the signal is hardly distinguishable from the background, and data are still being collected.

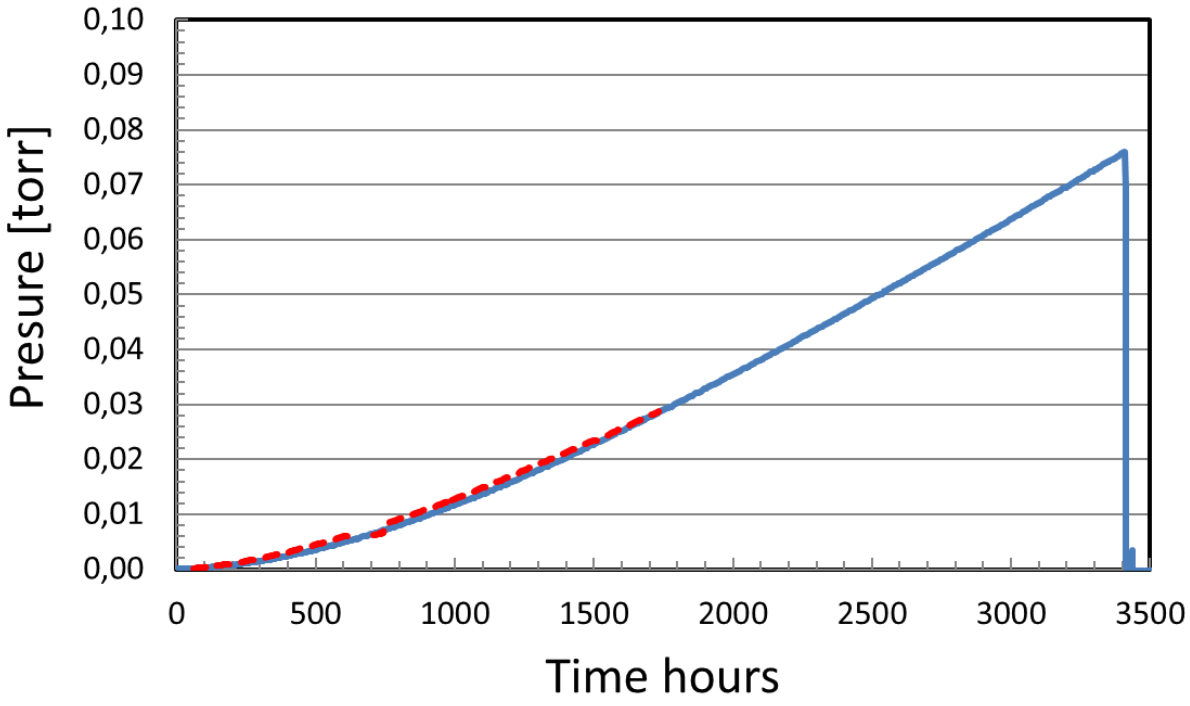

Fig. 3-6. *Current results from Main 3: The blue solid curve is the background and the red dashed curve displays the data for the diamond-scratched copper. The horizontal axis has been shifted to a common origin for the starting time. Data are the same as in Fig. 3-5, including the logging interruption.*

3.3 Surface analyses of copper

3.3.1. Free-standing vessels

The main analysis method was XPS applied to copper. We present results obtained for samples kept for a long time in the free-standing vessels and also for copper samples taken from Main 2. Since our focus lies on oxidation products, the outcomes of XPS as to its copper Auger spectrum are the most important, and these results are presented in section 3.3.1 and 3.3.2.

Fig 3-7 gives an overview of the XPS spectra obtained for the copper samples that have been exposed to water in the free-standing setups. In addition to the strong XPS peaks of copper, there are contributions by carbon, nitrogen and oxygen to be seen. Moreover, there are also Auger spectra of the most abundant elements where that of copper is the strongest. For this choice of radiation (Al $K\alpha$) these are found in the range 545-750 eV (Cu), ~980 (O) and 1200-1250 eV (C), respectively.

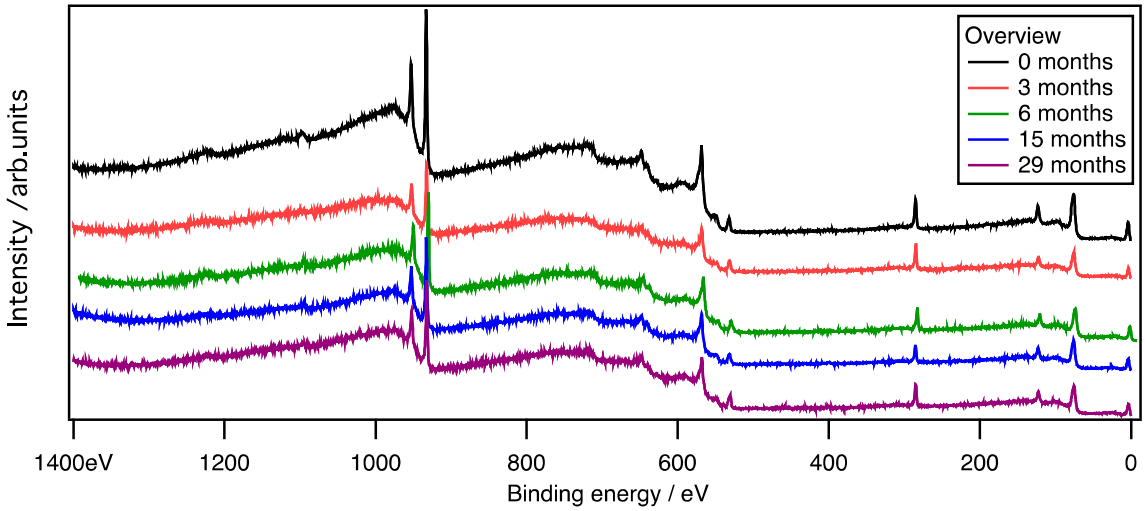

Fig. 3-7*. Overview XPS spectra of the copper samples after 0, 3, 6, 15 and 29 months. The 0-month sample is copper directly from the final purification step, after which samples were stored in water for various times.*

The strongest contributions from copper are found as two XPS peaks as shown in detail in **Fig. 3-8a**. These are peaks emanating from Cu *2p* states, being split from spin-orbit coupling. Even as being deeply lying states, they are sensitive to chemical bonding to some extent. In particular, there is a "channel" to *3d*-levels if these are not completely filled. Therefore, if copper were in the Cu(II) state, with a $3d^9$ configuration, each *2p* peak would carry a broad satellite structure at higher binding energy. Thus, the presence of CuO would clearly show up in two ways; the strong Cu *2p* peaks would appear with a chemical shift towards higher binding energy (approximately by 2.3 eV) and each one would be accompanied by a broad satellite towards higher binding energy (Boman et al. 2014). On the other hand, both Cu_2O and copper metal itself have a $3d^{10}$ configuration and their *2p* spectra differ too little to be distinguished from one another within the resolution of the instrument. Thus, these XPS spectra cannot directly reveal whether the sample is pure copper, pure Cu_2O or copper with some superficial Cu_2O.

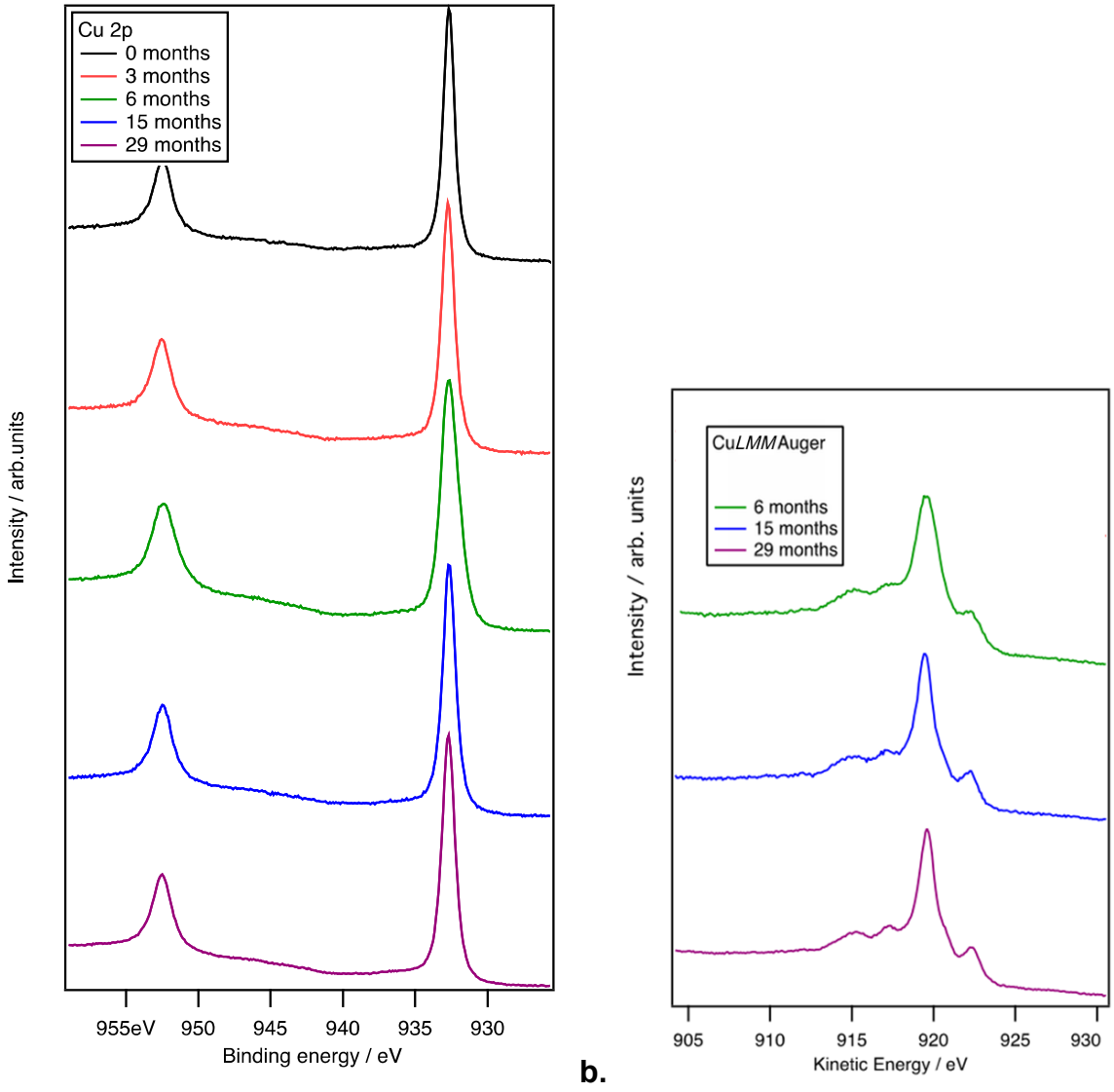

Fig. 3-8a-b. *(a) XPS Cu 2p spectra of copper samples after various exposure times. (b) Spectra of Cu $L_3M_{45}M_{45}$ for corresponding specimens as in 3-4a (from scanning the region around 570 eV of binding energy in the XPS overview). The energy is here expressed as increasing kinetic energy of the electrons.*

To discern Cu_2O deposited onto a copper surface, AES (spectra obtained from the XPS instrument by scanning the ~550-580 eV range of binding energy) was used. This more thorough analysis was initiated only from the 6 months' sample and implemented onwards. As can be seen from **Fig. 3-8b**, the Auger Cu $L_3M_{45}M_{45}$ spectra recorded after 6, 15 and 29 months all seem to be identical. As demonstrated in Boman et al. (2014, Fig. 5-11a), the spectrum did not change after heavy sputtering where pure copper is definitely reached.

For recording all the spectra, a special transference capsule was used and care was taken for substantially decreasing the delay between opening of the experiment vessel (glove box) and making the surface analysis (spectrometer), while no contact occurred with air in between. The successful effect of these latter precautions is obvious from the quality of the spectra. As was commented upon in Boman et al. (2014) that covered the first free-standing samples, the contribution of copper(I) oxide (Cu_2O) would have yielded a broad feature with its maximum

in kinetic energy at 917 eV (Panzner et al. 1985). Even after more than two years there is no such indication. **Fig 3-9** illustrates clearly the spectral changes in a series of sputterings of an oxide-covered copper surface until only pure copper is revealed (Cu L_3VV= Cu $L_3M_{45}M_{45}$).

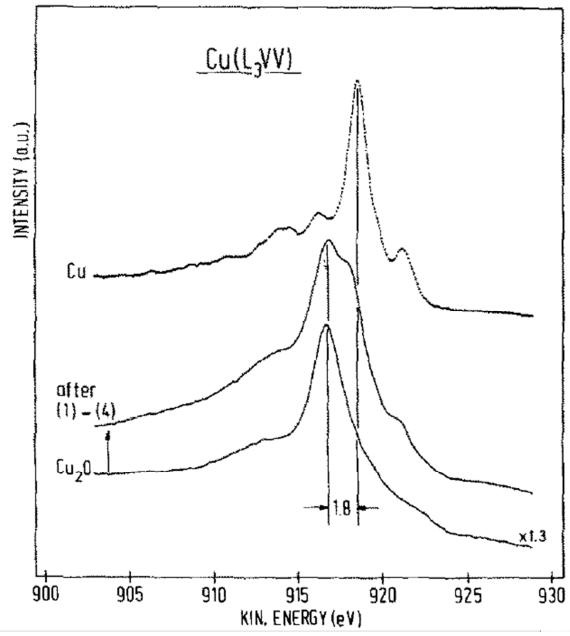

Fig. 3-9. *Comparative Auger spectra of Cu_2O and Cu, the latter obtained after sputtering a copper surface covered by the oxide and eventually exposing copper (Panzner et al. 1985).*

In addition, spectra were taken of the O *1s* contribution, expected to appear as a single peak. The outcome is more complicated, as illustrated in **Fig. 3-10a** The position of O *1s* for unbound elemental oxygen is 543 eV(Attwood 1999) but appreciably lower for oxides. A broad feature seems to be attributable to two dominating contributions centred at roughly 531 and 533 eV for all the investigated samples which indicates that oxygen is chemically bound in the same way as the electronegative part in more than one species. The 533 eV contribution has been attributed to superficial water (Cano 2001). That water may occur adsorbed is not surprising since the metal has been immersed in it. That the 531 eV peak should belong to $Cu(OH)_2$ (Chavez and Hess 2001, Park et al. 2011) can hardly be valid here, for no Cu(II) satellites were observed in the Cu *2p* spectra. It is more likely to belong to OH_{ads} (Andersson et al. 2008).

Noteable are the small peaks at 528 and 538 eV for the 6 and 15 months' samples. These might be attributed to *3d* contributions of antimony, but with energies as if in *unbound* form (Attwood 2000) which is surprising. This denotation rests upon their positions and the magnitude of their spin-orbit coupling splitting. Antimony should in water rather be found as an SbO^+ species. However, while the spectra from 6 and 15 months are largely identical, there is a pronounced change found for 29 months. The first couple of peaks attributed to Sb *3d* are now gone while the new couple remain. The intensities are larger, and now it is possible to see weak lines at 34-35 eV, typical of Sb *4d* (**Fig. 3-10a**, insert showing the doublet). It then seems that also the lines at 529.5 and 539.5 eV belong to antimony. The splitting is almost the same, so one interpretation might be that antimony occurs in more than one species and with different oxidation numbers. On increased time the binding energy of antimony then increases. It is natural to assume that antimony is bound to oxygen, and in Sb_2O_3 the binding energy of

the *3d* states is 530.3 and 539.6 eV, respectively, being about 1 eV larger for Sb_2O_5 (Garbassi 1980).

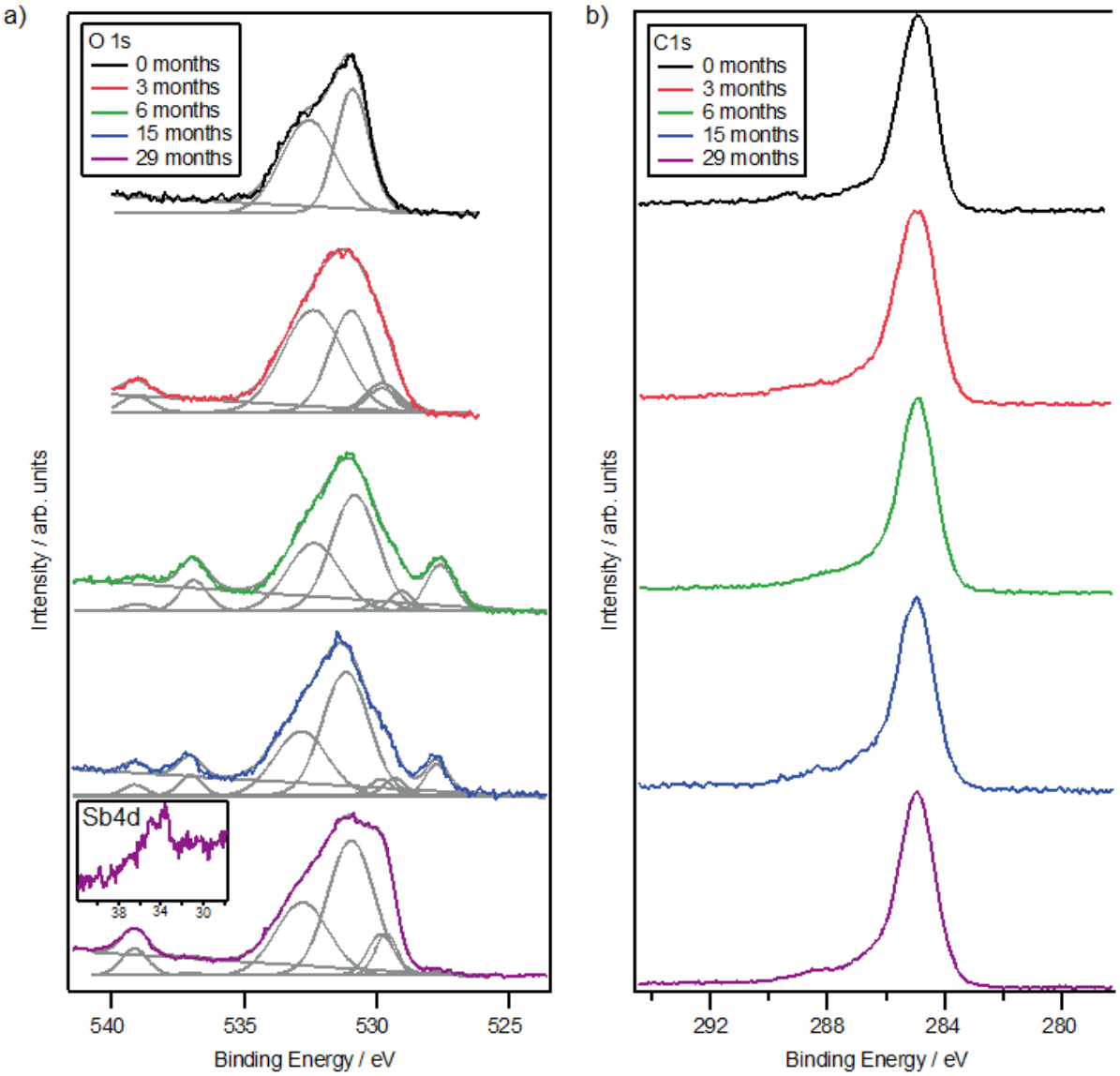

Fig.3-10a-b. *(a) XPS peaks recorded in the vicinity of the O 1s peak. The two upper spectra are less trustworthy due to less efficient protection against air. Sketched are also suggested deconvolutions into separate contributions (see text). The insert shows a low-angle contribution attributed to antimony (b) The XPS peak of carbon for the different samples.*

An iron antimonate ($FeSbO_4$) showed still higher values for the *3d* peaks, roughly 531 and 541 eV (Berry et al. 1987). It is interesting to note that in that case the oxygen O *1s* peak contribution, although the atom ratio O:Sb is relatively larger in the antimonate than in the oxides, was not large at all. It appeared only as a shoulder of the Sb $3d_{5/2}$ peak, thus only affecting the intensity ratio between the contributions of Sb $3d_{5/2}$ and Sb $3d_{3/2}$. The source of the antimony in our experiments (left on the copper from a water film) must be the glass beaker and not the added glass plate, deduced from the fact that these small peaks appeared also for a Main 2 experiment (*vide infra*) that was performed without an added glass plate. On

the whole, the amount of antimony is very low, considering the ppb content in the water (from ICP-MS, **Appendix D**), now concentrated in a thin film at the copper surface.

The deconvolution of spectra in XPS is an extremely tricky procedure. Specific contributions have to be determined out of a fixed sum, and the positions as well as the profile widths must be taken care of. Therefore, the choice presented in **Fig. 3-10a** must not be considered as the only possible solution. Care has been taken to include the value of the spin-orbit coupling of Sb *3d* contributions and the relative intensities of these peaks, but an uncertainly prevails. If there were an O *1s* contribution from Cu_2O, its position would be at 530.2 eV, an average value based on several measurements (Mariot et al. 1989). None of the indicated peaks seems to carry that position.

As to carbon, nothing spectacular is noted. The position of the C *1s* peak correlates simply to that of adventitious carbon from hydrocarbons always present. The C *1s* spectra are given in **Fig.3-10b** while the small Auger contribution (C *KLL*) is found in the overview spectrum at about 1200 eV but that contribution was not further analyzed.

3.3.2. Copper in Main 2 setup

The sample where the copper surface was first scratched by SiC paper before immersing the metal in water for 100 days was analysed by XPS.

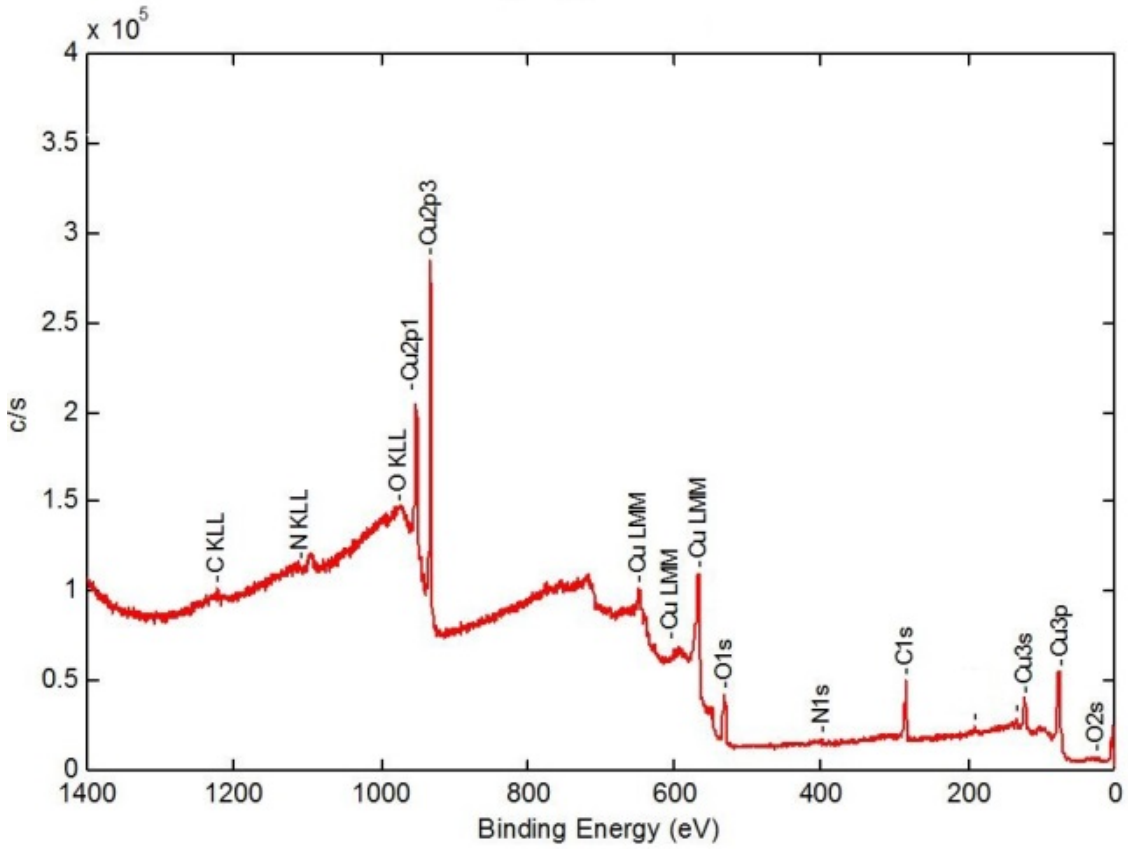

Fig. 3-11. *Overview XPS spectrum of the SiC-scratched sample from Main 2. (The weak features near O 1s emanate from the Auger Cu $L_2M_{45}M_{45}$.)*

Fig. 3-11 shows the XPS spectrum of the sample after exposure to water. There are no dramatic differences to the spectra given in **Fig. 3-7**, but some details are worth commenting on. There are some weak features between the peaks of C *1s* and Cu *3s*. The corresponding binding energies are 192 eV and 138 eV, respectively. A plausible interpretation is that both emanate from phosphorus (P *2s* and P *2p*, respectively).

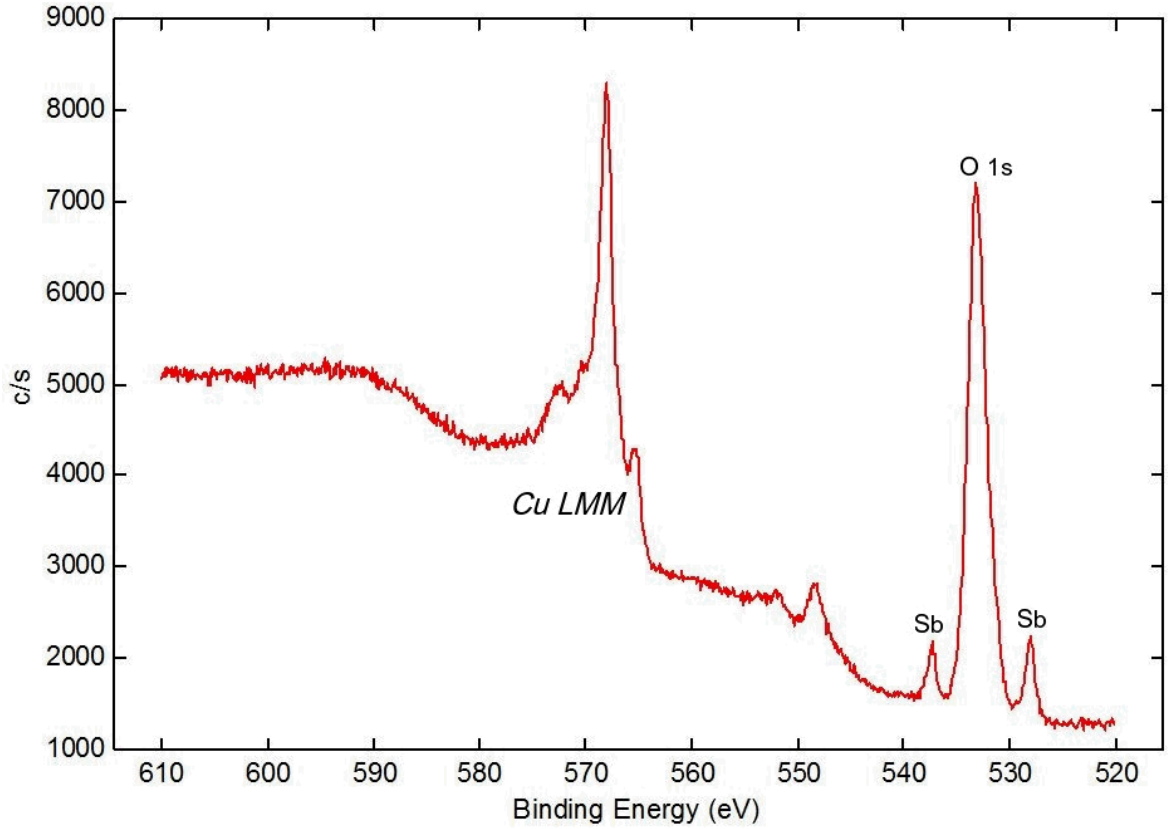

Fig. 3-12. *Part of the total spectrum for the SiC-scratched sample. Part of the whole Auger spectrum of copper is shown together with the oxygen O 1s peak together with contributions by antimony. The whole Auger Cu LMM range is broad, covering 545- 800 eV.*

In **Fig. 3-12** details of the total XPS spectrum are shown for an unsputtered surface. The Cu *LMM* spectrum, however not with the highest resolution, does not differ significantly from that of the unscratched samples of **Fig. 3-8b**. The scale is here expressed as binding energy in order to include also the part around the oxygen O 1s peak. In the Cu *LMM* spectrum, copper (I) oxide would have been revealed by a broad contribution centred near 570 eV (kinetic energy 917 eV; cf. **Fig. 3-9**). The conclusion that it is totally absent is a little uncertain due to inferior statistics.

The oxygen peak is, as was found in Boman et al. (2014, Fig. 5-9), accompanied by small peaks of antimony. The source must be the beaker glass for two reasons: A scratched copper sample not immersed in water did not show any antimony, and there was no other possible source present (no added glass plate) in this experiment with water.

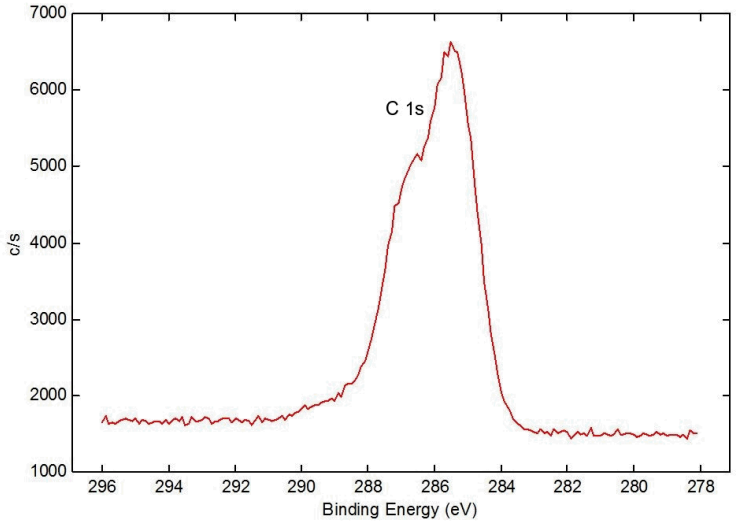

Fig.3-13 *XPS peaks of carbon from the SiC-scratched sample.*

A peculiar feature of the carbon spectrum of **Fig. 3-13** is that there are more than one contribution. The normal carbon peak comes from adventitious carbon (cf. Fig 3-10b). One explanation may be contributions from the SiC paper. Values given for SiC in the literature are 282.7 and 285 eV, the latter from C-C (Binner and Zhang 2001) as a result from contamination. Another carbon source may be from additives in the SiC paper in the form of organics containing carboxylic carbon (O-C=O). That such additives really are present was indicated in hydrogen desorption experiments where the presence of CO and CO_2 in the gas phase was established from mass spectrometry (QMS). These contributions are reflected in the high-energy shoulder and they might also affect the O 1s spectrum (Johansson et al. 2012).

These discrepancies as regards elements present compared with the spectra of polished and purified copper indicate that there are distinct additional contributions from the SiC paper. Another example is the detection of sulphur, as illustrated in **Fig. 3-14**.

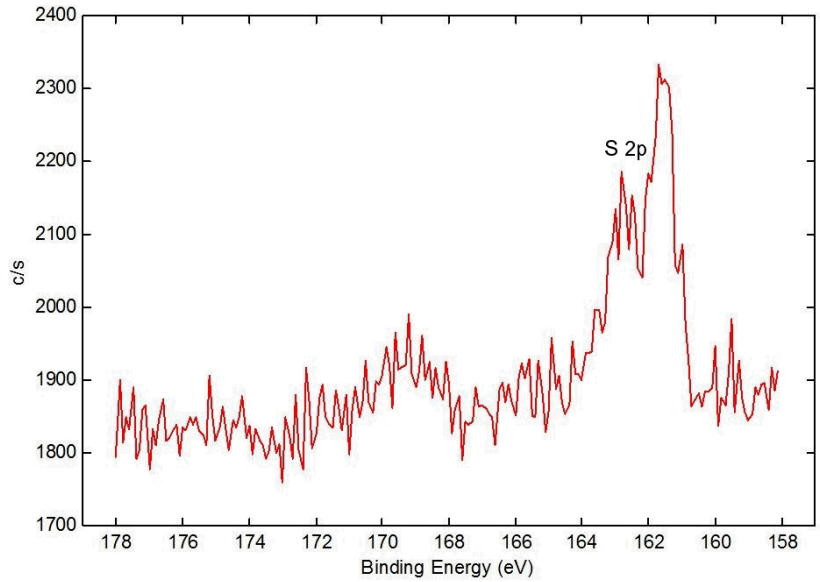

Fig. 3.14*. Weak peaks of sulphur, found for the SiC-scratched copper sample.*

3.4 Bulk analyses of copper: Hydrogen content

3.4.1. Fusion analysis

The samples that were investigated (with improved accuracy) are collected in **Table 3-3**. The copper quality was 99.9999% as regards bulk composition (Alfa Aesar). We measured the metal as received (pristine) as well as after electropolishing (EP) and subsequent purification steps (Boman et al. 2014). We include measurement of the 29 months' water exposure sample that had undergone these purification steps. Contrary to routine procedure for removal of surface oxide, the surface was not polished for any of these samples before the melting. The analysis certificates are found in **Appendix E**.

Experience from previous measurements shows that a large spread in the analysis figures is obtained if the sample sizes are too small, discussed in **Appendix E**. It might reflect a degree of inhomogeneity of the copper sheet or be an effect of decreased accuracy of the method. That was a problem in Boman et al. (2014, Section 5.2.4) and has now been overcome by increasing the mass up to 5-6 g. With ASTM E1010 as reference, contents of the order of 0.1 ppm can be measured. The conclusions concerning procedure drawn from the analysis results of Table 3-3 are:

- Heating alone at 600°C is efficient in removing hydrogen from pristine copper, from 0.7 to 0.06 ppm.
- The content decreases from 0.7 to 0.16 ppm by electropolishing (room temperature).
- The following step that encompasses heating in hydrogen is still more efficient, reducing it to 0.03 ppm, a value near the limit of detection by the method.

Electropolishing is an etching oxidation process (copper is the anode). If there exists an accumulation of hydrogen in the surface layer, that gets removed even at room temperature. Larger reduction is attained by further heating in hydrogen. An important fact is that heating in hydrogen does not increase the hydrogen content but rather the opposite.

Table 3-3. *Hydrogen content as determined by the LECO method (unpolished copper surface)*

Copper sample	Pristine	EP	EP + H_2 [a]	EP + H_2 [a] +ht [b] (400°C)	Pristine +ht [b] (600°C)	29 months
Hydrogen content (ppm)	0.7	0.16	0.03	0.03	0.06	0.09

[a] Hydrogen gas reduction at 300°C; [b] Hydrogen reduction followed by heat treatment at 400°C or 600°C

3.4.2. Hydrogen desorption

Heat treatments were carried out as previously, *i.e.* first by reducing the surface oxide layer (after electropolishing the sample in a diluted H_3PO_4 solution) in order to remove all oxygen from the surface. This treatment was performed at 300°C for one hour in a hydrogen atmosphere and has proven to work for samples with an oxide layer observable to the eye. During this annealing, hydrogen is expected to partially desorb from the bulk. Then, after cooling, the tube with the sample was evacuated to low pressures (below 10^{-7} Torr), where residual gas analysis is possible, and was further annealed at 400°C while logging the partial pressures of selected species (QMS).

Two processes were observable in untreated samples ("as received"), first a desorption which gives the highest partial pressure, probably from the surface, and then another desorption from the bulk which is a more prolonged process. These are clearly seen in **Fig.3-15**. For comparison, data for the corresponding heat treatment of two foils having experienced surface purification (Boman et al. 2014) are shown, one directly after purification and one after 6 months in ultrapure water. The partial pressures are very low for the latter two, and the noisy appearance illustrates that they lie at the verge of resolution by the equipment. Note that the mass of the 6 months' sample is 10 times smaller than that of the others.

All qualities show a gas desorption process that commences just after 400°C has been reached. (A small delay after heating change may occur.) Annealing of copper up to 600°C has shown that hydrogen is effectively desorbed in the temperature range 300-400°C with a high evolution rate at 400°C (See **Appendix E,** heating rate 1 K/min.). Hence, a treatment at this temperature effectively removes dissolved hydrogen from the bulk (and surface, if present), as is corroborated by the fusion analysis results given in 3.4.1.

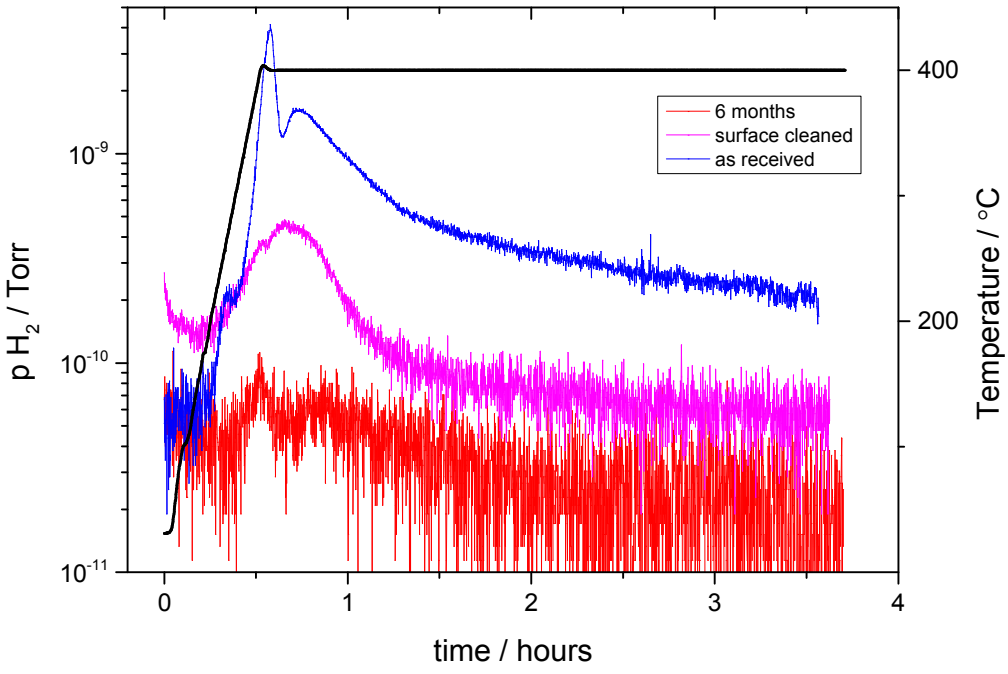

Fig. 3-15 *Pressure/temperature vs. time characteristics on heat-treating Cu foils of 99.9999% purity. One sample is "as received" from the supplier (blue), one has gone through a surface purification process (magenta), and one has after that been exposed to water for 6 months (red). The mass of the latter sample is 10 times smaller than that of the other two. The axis to the left on a logarithmic scale alludes to the data in colour. The applied temperature in black is read on the axis to the right (linear scale).*

3.5 Analyses on the near environment (water, glass)

3.5.1. Water phase in contact with copper

The water was analysed by ICP-MS, a method that can detect and determine very small amounts of elements dissolved. The main features of the technique were presented in Boman et al. (2014).

Six water samples representing a time span of 0-29 months (0, 1, 3, 6, 15, 29) have now been measured using a semi-quantitative method for scanning a majority of the naturally occurring elements. The element concentrations of the water samples generally tend to increase over time as depicted in **Fig. 3-16**. For each element (symbols arranged in alphabetical order), the respective concentrations are shown as histograms that are fading in colour tone as a function of increasing time.

Most elements seen in the water sample are probably a result of leaching from the glass container by the water itself or from the polymer tube used as sample vessel for measuring. The presented concentrations are rather uncertain due to the large concentration differences between several elements and the one point calibration, as well as to the problem of compensating for interferences by some elements (e.g. K, Ca and P). This uncertainty should however be equal for all samples since they were measured using the same calibration and instrumental settings and with a relatively similar matrix for all the samples. Therefore, the presented data can be used for comparison between samples in time and within each element, but it should be noted that the "real" concentration could vary substantially for elements that suffer from interferences and/or are present in very high concentrations (>100µg/L) or in very low concentrations (<0.1µg/L). A comparison to earlier measurements (see previous report) was also made to ensure that no substantial difference in concentration occurred due to storage. The samples exhibited quite comparable levels to those of previous measurements. Therefore, the data of **Fig. 3-16** most likely present a valid comparison between time points. Detailed numerical values may be found in **Appendix D**.

The elements that occur with the highest contents (please note the logarithmic scale) most likely emanate from leaching of the glass (*e.g.* Al, B, K, Na, Si; high-lighted in the table of Appendix D). Zinc and magnesium are borderline cases, being elements that easily may contaminate samples from the surrounding environment. All concentrations are "low", remembering that 1 ppb (= 1000 ng/L) corresponds to the figure 3 on the logarithmic horizontal scale.

After exposure of the copper samples to water during 29 months, the copper concentration has reached about 25 µg/L (Table 3-4). As an illustration of the very small magnitude, that value corresponds to $4 \cdot 10^{-7}$ M Cu which is only a factor of four times the hydrogen ion molar concentration in pure water, in other words a very low concentration.

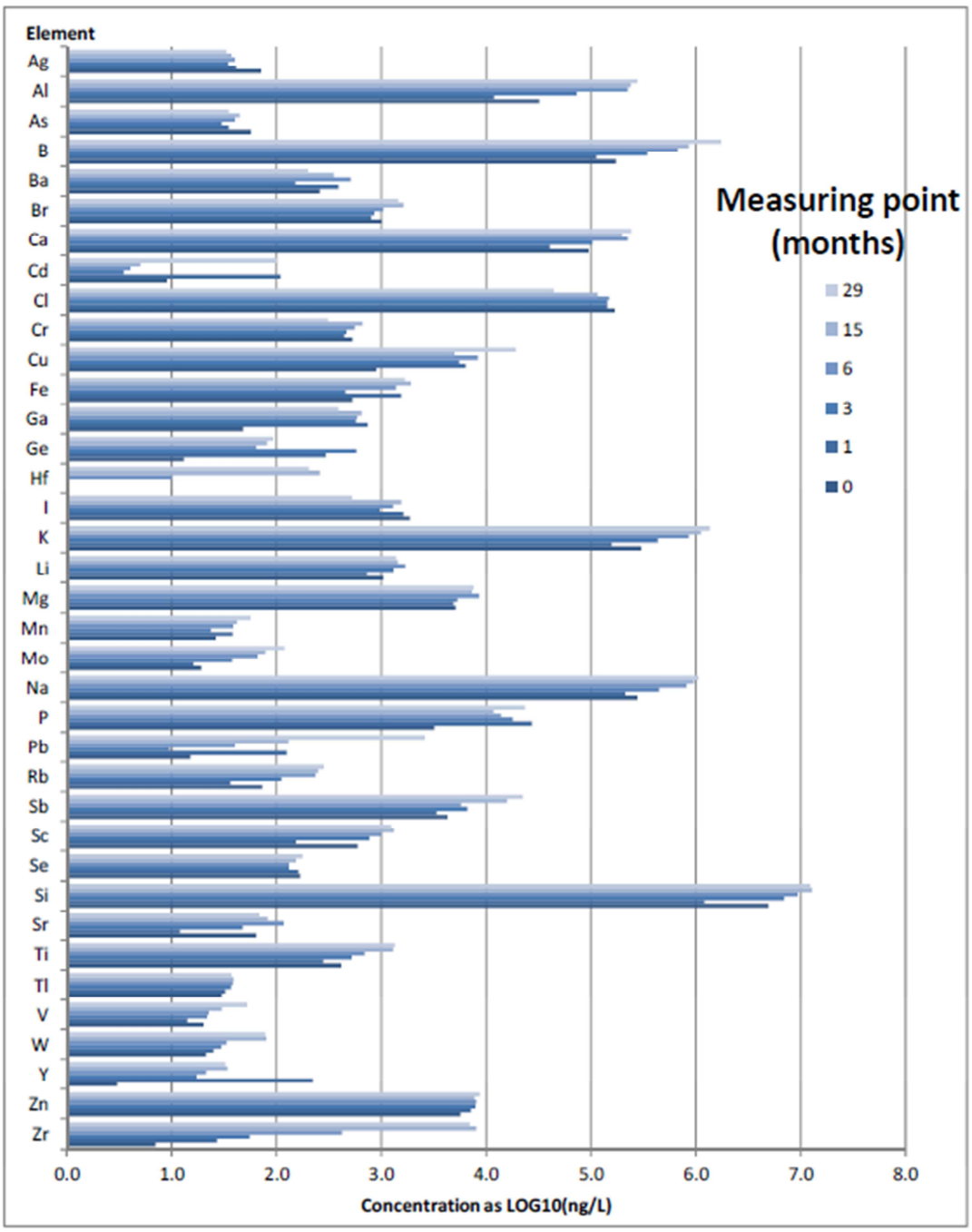

Fig. 3-16. *Overview of elements in the water phase investigated by ICP-MS that have a concentration of 1 ng/L or more. The logarithmic presentation means a tenfold difference in concentration between each scale division on the horizontal axis.*

Table 3-4 presents an example of the most recent results from ICP-MS, concerning the 29 months' sample and those of scratched copper. For confirmation that the values were not severely marred by systematic errors, two isotopes of copper were measured and the concentrations scaled according to isotope abundance. The corresponding scaling procedure was also applied to iron, normally determined from ^{57}Fe. Even in that case, however, special care was taken to eliminate errors, in particular to avoid contamination by $^{40}Ar^{17}O$ (Boman et al. 2014).

It may be noted that the scratched samples, although exposed a relatively short time to water (see section 3.1), show a copper content that is comparable to that of the long-term sample. One interpretation is that the scratching process yields minute copper particles that are dispersed (or have a large solubility) and enter the plasma, more pronounced for scratching by diamond that is harder. On the other hand, the diamond-scratched sample showed a high concentration of zinc, probably because natural diamond was used. Due to the short exposure time of the glass to water, the contents of zinc and antimony are low for the SiC-scratched copper (antimony comes from the beaker glass). The high content of aluminium probably emanates from the SiC-paper used. When sintering the silicon carbide, Al_2O_3 is commonly added (Sciti and Bellosi 2000).

Table 3-4. *Selected analysis results from ICP-MS of the water phase for various isotopes. Concentrations are given in μg/L (ppb)*

Sample	**^{24}Mg**	**^{27}Al**	**^{63}Cu**	**^{65}Cu**	**^{66}Zn**	**^{121}Sb**	**^{57}Fe**
29 months	9.2	329.9	23.6	25.7	13.9	27.1	1.4
Scratched (SiC)	9.8	248.9	18.6	20.0	1.4	0.4	1.7
Scratched (diamond)	5.2	33.9	67.6	65.7	107.1	0.6	1.5

As described in the previous recapitulation of the technique above, a more precise method to measure Cu levels in the water samples was also used in addition to the semi-quantitative method. The results of those measurements as plotted in **Fig. 3-17** seem to give an almost linear relationship between time and Cu concentration, assuming that the point at 15 months is ignored as an "outlier". However, that assumption cannot be strictly made and is misleading, considering that the measurement at 29 months could equally well be an outlier as a result from contamination during sample handling and analysis, from which the relationship looks more parabolic instead. Since there are no technical replicates made for each sample, it is improper and pointless to draw any conclusions about the more exact relationship between time and Cu concentration. Further measurements would have to be made in order to ascertain which, if any, data point is an outlier.

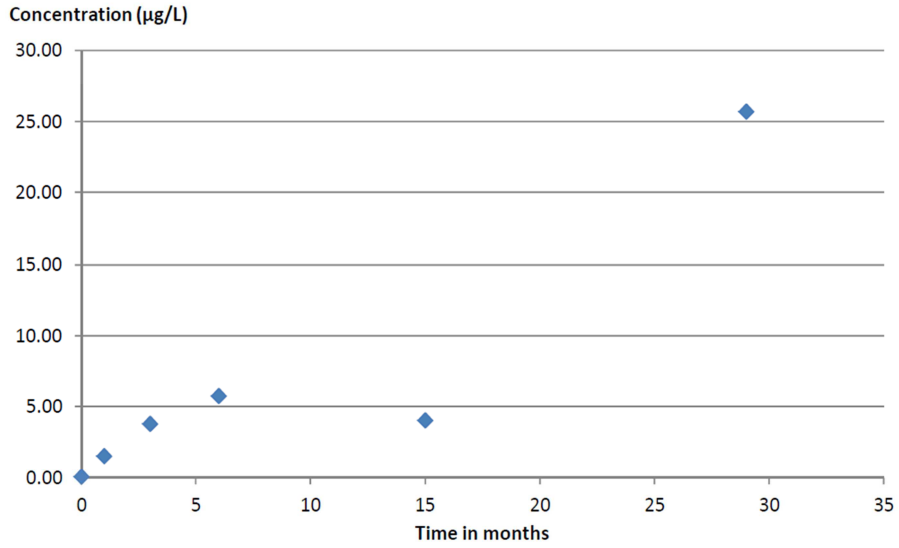

Fig. 3-17. *Time dependence (discrete measurements) of the copper concentration in the water phase.*

3.5.2. Glass in contact with water

The use of the XRF technique for determining copper in the glass plates that accompanied the copper in the water was described in Boman et al. (2014, Appendix D4). The beaker itself could not be analysed in the spectrometer for geometrical reasons. The XRF technique cannot determine in what form copper occurs or its distribution, *i.e.* whether the signal emanates from a surface layer or is a bulk property. **Table 3-5** shows the analysis results where the amount of copper is expressed as a fictitious thickness of a copper layer that corresponds to the intensity recorded. These analyses were made for the free-standing vessels, now including previous results as well. The precision of the data is in the order of 30% and there are indications (from ICP-MS) that the spread between different glass plates is larger than that, thus affecting the accuracy. The data show no obvious trend with time, *i.e.* one cannot tell whether the copper content increases (surface deposition) or decreases (glass leaching).

Table 3-5. *Copper content in glass plates exposed to water in beaker with residing copper.*

Exposure time	3 months	6 months[a]	15 months	29 months
Thickness (nm)	0.00	0.03; 0.05	0.04	0.03

[a] Measured from two directions of the same plate

3.6 Miscellaneous complementary techniques

3.6.1. Scanning AES and SEM

Copper foil that had been in water for 6 months was investigated by scanning electron beam AES. **Fig. 3-18 a** shows that the copper surface, as seen in the SEM of the scanning Auger spectrometer, is very smooth with very narrow grain boundaries. **Fig 3-18 b** shows ultrapure copper after the first purification step, the electropolishing, after which the surface is covered with a thin layer of oxides later removed by hydrogen treatment before the experiments.

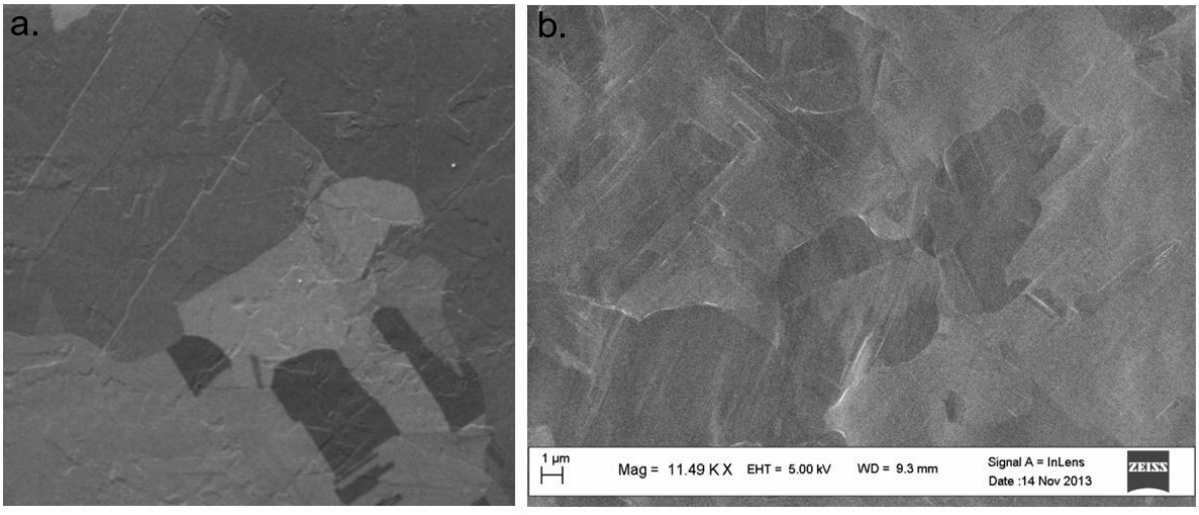

Fig. 3-18 a-b. *(a) A SEM micrograph of the surface of the 6 months' sample from the scanning Auger spectrometer; (b) SEM picture of ultrapure copper after electropolishing, before the experiments. Different orientations of the copper grains yield the contrast.*

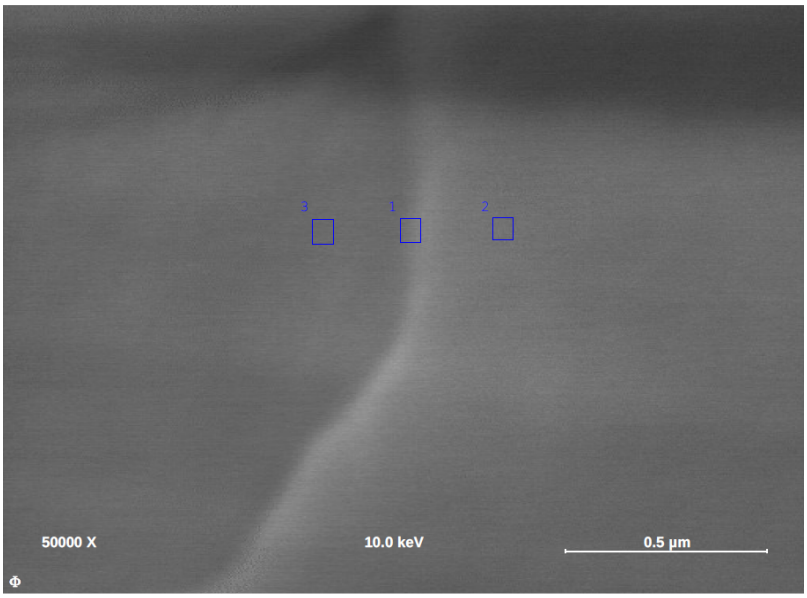

***Fig.3-19**. SEM picture showing the copper microstructure with spots where the surface was analysed.*

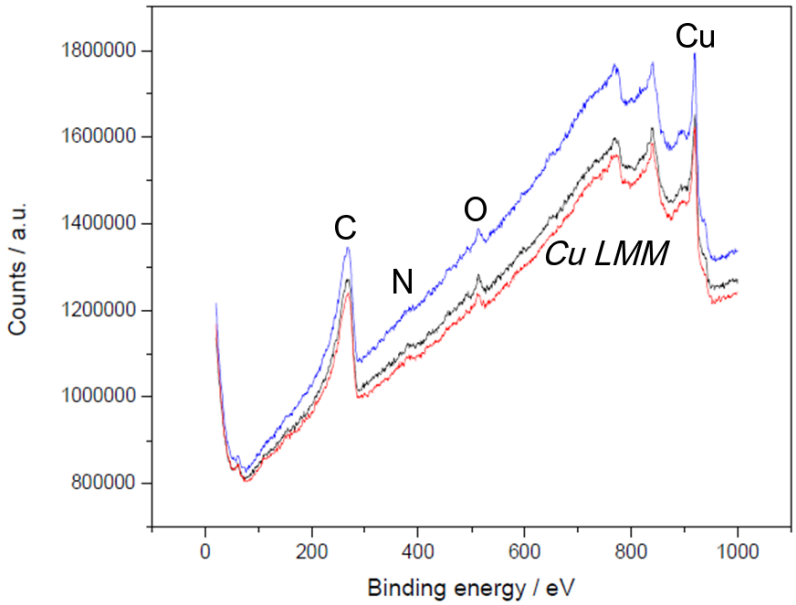

***Fig.3-20.** Corresponding AES data from the spots 3-1-2 chosen in Fig.3-17 (number 3-blue, 1-black, 2-red). The middle curve (1-black) comes from the point at the grain boundary. The energy is here given as binding energy for an easy comparison with values from XPS spectra (See **Fig. 3-11** for proper denotations).*

Electron-beam AES was used in order to disclose inhomogeneity, in particular signs of corrosion attacks at the grain boundaries where then oxide would form preferentially. That could not be done by XPS where the analysing ray is much wider, goes deeper and cannot be controlled as to where it hits. The experimental strategy is illustrated in **Fig.3-19** where spots were chosen, either on a grain boundary or at adjacent areas. The spectra corresponding to these very spots are given in **Fig.3-20**, showing that the copper surface is fairly clean (sample container was opened in air before loading). More important, there is no accumulation of contaminants at the grain boundary (middle trace in black from point 1). The peaks are

attributed to carbon, nitrogen, oxygen and copper. The peak shapes and background characteristics are different from those in XPS because only electrons are involved with this technique, not X-ray photons.

The measurement procedure showed that adventitious contamination by carbon was continuously introduced within the spectrometer (explaining the abnormal intensity of the C *1s* peak), easily monitored on waiting some minutes directly after a short sputtering. Since the extra amount is minute, the strong response illustrates the high sensitivity of the method. Iterative sputtering tests showed the same phenomenon concerning the spectra, and the corresponding SEM mode showed (no pictures available) how the etching of the copper proceeded by consecutive sputtering operations, creating pronounced edges of the grains.

3.6.2. Transmission electron microscopy

Transmission electron microscopy (TEM) may be used in two different ways, either for studies of the absorption through thin samples or for electron diffraction. In both cases very thin samples are needed because of the strong absorption by electrons. In the absorption mode, very high resolution may be obtained and the grade of crystallinity and occurrence of dislocations can be studied.

For making a TEM micrograph (**Fig. 3-21**), a thin slice of copper was ion-beam milled out of a foil of the 99.9999% quality used. It was thin enough to make it electron-beam transparent, but platinum was deposited on the copper as a backing before the thinning process which protects the copper surface from ion damage. The surface shown is the interface Cu/Pt. Voids that could contain H_2 were neither observed nor expected, considering the low hydrogen content.

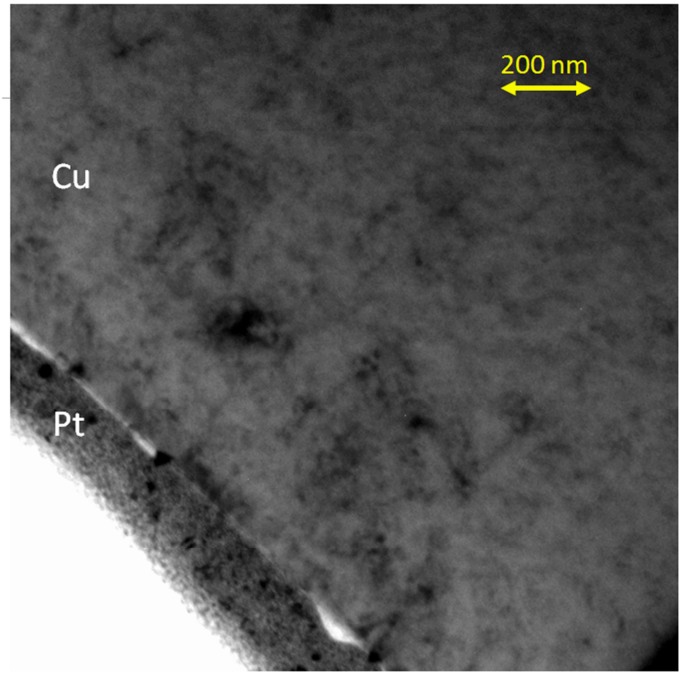

***Fig. 3- 21**. A TEM micrograph of ultrapure copper, purified in steps as described in Boman et al. (2014). The thin copper slice is situated on a platinum backing.*

4. Discussion and conclusions

We have continued the work already reported on (Boman et al. 2014) along two lines: First of all, the time for the long-term experiments of copper in water has been extended, now including from 15 months up to 29 months. These samples were kept for the study of *copper oxidation* by various chemical methods, a well-defined way to establish a true picture of a corrosion process since the existence of hydrogen production alone may be misleading.

Secondly, renewed experiments have been performed concerning the pressure measurements, urged from the fact that hydrogen as a product of *water reduction* (from a corrosion process) had to be distinguished from other sources of production. The kernel of the problem was how to bring down the background level of hydrogen, knowing that stainless steel is a source that cannot be circumvented except for totally redesigning the equipment – which is outside the scope of the project. Considering the low degree of oxidation products, we have encountered a challenging problem how to decrease the background so much that the corresponding calculated hydrogen contribution from a corrosion process could be discerned. Extensive heat-treatments have brought down the hydrogen emission from the steel to a very low level, in line with the best values reported in the literature. In addition to the work on reducing the background, a new design was adopted for the palladium membrane fitting so that no hydrogen flow was possible other than between the reaction chamber and the compartment with the pressure gauges. These latter were changed to improve the accuracy because of much lower outgassing, meaning a decreased background level from this exchange.

A few short-term experiments were made with the modified equipment where the surface was modified by manual scratching, with the idea that copper that had been roughened at the surface might change its reactivity through the introduction of dislocations or even by the creation of nano-particles.

As before, the copper has been investigated by XPS and AES. The Auger Cu *LMM* spectrum showed, even after 29 months' exposure of the copper to water, only the features of pure copper. In fact, there is no evolution in time compared to the previous samples when aiming at the only probable surface product, Cu_2O, which is unambiguously detectable by this technique. Neither were there any sign of contaminants accumulated in the grain boundaries as established with an electron Auger spectrometer designed for spot analysis. The antimony and accompanying oxygen-containing species at the surface, as detected by XPS, must be discarded as associated with a corrosion process: The source of antimony is the glass beaker that is being leached by the water, however to a low concentration (ppb level). The antimony species are present in that water (from ICP-MS) and are probably not deposited onto the copper but only dragged out in a thin water film that adheres to the metal surface all the way into the spectrometer. Thus they are easily removed by gentle sputtering.

As mentioned in section 2.2, previous measurements of hydrogen content in copper (Boman et al. 2014) were hampered by inferior handling. The main drawbacks with the LECO method of fusion are that it craves gram-size samples and cannot use the very same sample again for analysis. Renewed LECO measurements of bulk hydrogen, complemented by desorption studies, showed that the hydrogen content is low . Contrary to what has been suggested, the purification steps (electropolishing + hydrogen reduction) strongly reduce the hydrogen content. The final treatment at 400°C, where most of hydrogen desorption occurs, obviously guarantees a continued low hydrogen content. Studies by TEM corroborated these findings.

For the electropolished copper that has undergone exposure to water for a prolonged time span – up to 29 months – the following facts may be summarized as the outcome of analyses:

- The copper Auger spectra from 6, 15 and 29 months are identical and show no detectable Cu_2O, only pure copper.
- There is a tendency of increased copper concentration by time in the water but it is still very low (~10^{-7} M).
- There is no tendency of increased copper in (or on) the added glass plates by time.
- The low hydrogen content of the copper obtained through the purification does not increase on exposure to water.
- The pressure increase is hardly discernible from the background that, compared to Boman et al. (2014), has been lowered considerably through the new design and harsher heat treatments.

The attempts to change the surface structure of the copper have yielded results in the pressure monitoring that are difficult to evaluate and interpret. The two substances used for scratching, SiC and diamond, yielded different results. The experiment with silicon carbide showed a pressure increase compared to the background while no significant deviation from background value could be recorded from the diamond-scratched copper. To obtain a better basis for the evaluation of the experiment, it needs to be repeated. ICP-MS showed that the water from the SiC-scratched specimen from a limited exposure contained enhanced concentrations of copper and aluminium, of the same magnitudes as from the 29 months' sample of polished copper. The Al-content found by ICP-MS is an indication that the use of silicon carbide has created contamination of the sample. The enhanced copper concentration may at least partly be an effect of minute copper metal particles having come off mechanically by the scratching. XPS disclosed the presence of elements (P, S) that cannot come from the glass or the copper, and traces of species containing bonds C-O were indicated.

The scratching of copper by SiC seems to influence the outcome of the experiment:

- Concentrations in water of aluminium and copper get enhanced, and both phosphorus and sulphur appear on the copper surface (contaminations).
- The hydrogen evolution seems enhanced.
- There is a distinct change of carbon species at the copper surface – but no Cu_2O can be discerned.

The scratching of specimens by diamond yielded less dramatic effects:

- Concentrations in water (immersed for six days) of copper and zinc get enhanced, largely an artefact from the material and handling.
- The hydrogen evolution does not significantly deviate from the background.
- (No XPS data available since the experiment is still running)

On the basis of these experiments, no explanations can be offered why the SiC-scratched copper behaves differently from a flat copper surface. Moreover, if surface conditions were to determine the outcome, the question remains why the diamond-scratched sample does not yield the same effects. However, scratched samples cannot be compared in a valid manner as long as the parameters of such treatments are not perfectly controlled and made reproducible.

In these cases, however, we strongly suspect that SiC particles somehow take active part and change the reactivity. The formation of local galvanic cells is one alternative that we have not been able to investigate.

Since copper corrosion is revealed unambiguously only from its oxidation products, either by a deposition onto the copper or into the water phase, the conclusion prevails that there are no obvious signs of a significant corrosion process involving copper even after 29 months at 50°C. In fact, the corresponding Auger spectrum (Fig. 3-8b) has the best quality of them all, due to a very rapid transference of the sample to the spectrometer, and the interpretation is indubitable. Although at the same time the copper concentration in the water has increased with residing time, we cannot rule out leaching from the beaker glass as part of the observed enhancement. Even if all dissolved copper were to emanate from the copper metal, the effect is very small.

Autocatalytic dissociation of water on a copper surface has been claimed (Andersson et al. 2008) that might be able to yield evolution of hydrogen on the simultaneous formation of a surface OH-species as a monolayer. In a first stage, the dissociation leaves adsorbed OH and H that very well may recombine and leave the surface. That study operated with gaseous water which means that the surface energy term would be relatively more important than in liquid water. Cu_2O is thermodynamically still more stable under such conditions and would be expected to form. A monolayer of this oxide is without doubt detectable by Auger spectroscopy; none was found.

5. Acknowledgements

This work was financed by the Swedish Nuclear Fuel and Waste Management Co. but the planning, strategy, experimental solutions and conclusions have not been influenced or restricted by that fact.

The work rests to a large extent on the possibility to have the equipment refurnished and the analyses made with the highest accuracy. Moreover, we have relied on the easy access of the facilities of the Ångström Laboratory. We thank Jonas Ångström for the skilful help with preparation of copper samples and Jan Bohlin for excellent workmanship in machining the stainless steel equipment.

Finally we are indebted to Ingvar Bernhardsson and coworkers at the Degerfors Laboratory for their willingness to deviate from routine practice in their hydrogen analyses to conform to our wishes concerning sample preparation.

References

Andersson K, Ketteler G, Bluhm H, Yamamoto S, Ogasawara H, Pettersson L G M, Salmeron M, Nilsson A, 2008. Autocatalytic water dissociation on Cu(110) at near ambient conditions. Journal of the American Chemical Society 130, 2793–2797.

Attwood D T, 1999. Soft X-rays and extreme ultraviolet radiation: principles and applications. Cambridge: Cambridge University Press.

Berry F J, Holden J G, Loretto M H, Urch D S, 1987. Iron antimonate. Journal of the Chemical Society, Dalton Transactions, 1727–1731.

Bills D G, 1969. Ultimate pressure limitations. Journal of Vacuum Science and Technology 6, 166–173.

Binner J, Zhang Y, 2001. Characterization of silicon carbide and silicon powders by XPS and zeta potential measurement. Journal of Materials Science Letters 20, 123–126.

Boman M, Ottosson M, Berger R, Andersson Y, Hahlin M, Björefors, F, Gustafsson T, 2014. Corrosion of copper in ultrapure water. SKB R-14-07, Svensk Kärnbränslehantering AB.

Cano E, Torres C L, Bastidas J M, 2001. An XPS study of copper corrosion originated by formic acid vapour at 40% and 80% relative humidity. Materials and Corrosion 52, 667–676.

Caravella A, Hara S, Drioli E, Barbieri G, 2013. Sieverts law pressure exponent for hydrogen permeation through Pd-based membranes: couples influence of non-ideal diffusion and multicomponent external mass transfer. International Journal of Hydrogen Energy 38, 16229–16244.

Chavez K L, Hess D W, 2001. A novel method of etching copper oxide using acetic acid. Journal of the Electrochemical Society 148, G640–G643.

Flanagan T B, Lynch J F, Clewley J D, von Turkovich B, 1976. The effect of lattice defects on hydrogen solubility in palladium: I. Experimentally observed solubility enhancements and thermodynamics of absorption. Journal of the Less Common Metals 49, 13–24.

Garbassi F, 1980. XPS and AES study of antimony oxides. Surface and Interface Analysis 2, 165–169.

Holleck G L, 1970. Diffusion and solution of hydrogen in palladium and palladium–silver alloys. Journal of Physical Chemistry 74, 503–511.

Hultquist G, 1986. Hydrogen evolution in corrosion of copper in pure water. Corrosion Science 26, 173–177.

Hultquist G, Szakálos P, Graham M J, Belonoshko A B, Sproule G I, Gråsjö L, Dorogokupets P, Danilov B, AAstrup T, Wikmark G, Chuah G-K, Eriksson J-C, Rosengren A, 2009. Water corrodes copper. Catalysis Letters 132, 311–316.

Hultquist G, Graham M J, Szakálos P, Sproule G I, Rosengren A, Gråsjö L, 2011. Hydrogen gas production during corrosion of copper by water. Corrosion Science 53, 310–319.

Johansson J, Blom A, Chukharkina A, Pedersen K, 2015. Study of H_2 gas emission in sealed compartments containing copper immersed in O_2-free water. SKB TR-15-03, Svensk Kärnbränslehantering AB.

Johansson L-S, Campbell J M, Hänninen T, Ganne-Chèdeville C, Vuorinen T, Hughes M, Laine J, 2012. XPS and the medium-dependent surface adaptation of cellulose in wood. Surface and Interface Analysis 44, 899–903.

Jones D A, 1992. Principles and prevention of corrosion. New York: Macmillan.

Mariot J-M, Barnole V, Hague C F, Vetter G, Queyroux, F, 1989. Local electronic structure of Cu_2O, CuO and $YBa_2Cu_3O_{7-\delta}$. Zeitschrift für Physik B Condensed Matter 75, 1–9.

O'Hanloon J F, 2003. A user's guide to vacuum technology. 3rd ed. Hoboken, NJ: Wiley.

Panzner G, Egert B, Schmidt H P, 1985. The stability of CuO and Cu_2O surfaces during argon sputtering studies by XPS and AES. Surface Science 151, 400–408.

Park C D, Chung S M, Xianghong Liu, Yulin Li, 2008. Reduction in hydrogen outgassing from stainless steels by a mnedium-temperature heat treatment. Journal of Vacuum Science and Technology A26, 1166–1171.

Park J-Y, Lim K-A, Damsier R D, Kang Y-C, 2011. Spectroscopic and morphological investigation of copper oxide thin films prepared by magnetron sputtering at various oxygen ratios. Bulletin of the Korean Society of Chemistry 32, 3395–3399.

Sciti D, Bellosi A, 2000. Effects of additives on densification, microstructure and properties of liquid-phase sintered silicon carbide. Journal of Materials Science 35, 3849–3855.

Szakálos P, Hultquist G, Wikmark G, 2007. Corrosion of copper by water. Electrochemical and Solid State Letters 10, C63–C67.

Ward T L, Dao T, 1999. Model of hydrogen permeation behavior in palladium membranes. Journal of Membrane Science 153, 211–231.

APPENDIX A

Details concerning the reconstruction of the assemblies

A 1. Construction of the new lid

The lid was made from a solid rod of 316L steel with a CF-63 connection to the lower chamber. The upper part has a CF-38 connection to the vacuum chamber. Inside the CF-38 there is a Swagelok VCR ¼" fitting for the Pd membrane. The membrane was mounted in the gasket retainer assembly. When the gasket is tightened, the Pd membrane gets pressed towards the body welded on the lid. The VCR assembly was leak-detected with helium. This VCR–Pd fitting acts as a hydrogen filter. The external CF-38 is the outer seal. This construction gives no air contact of the Pd membrane.

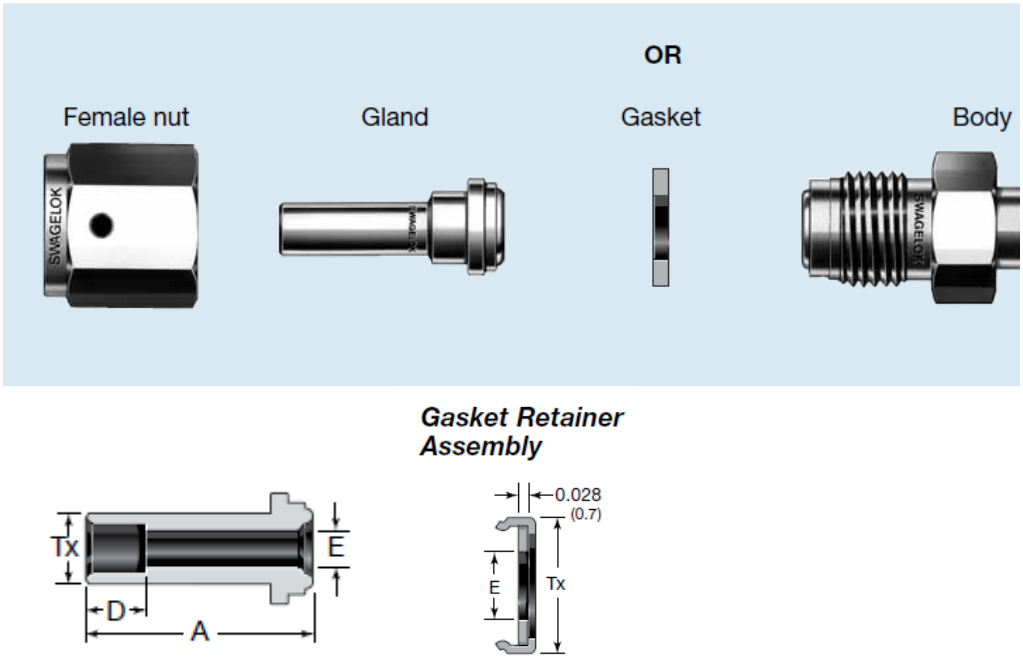

Fig. A-1. *The principle of the he VCR fitting from Swagelok*

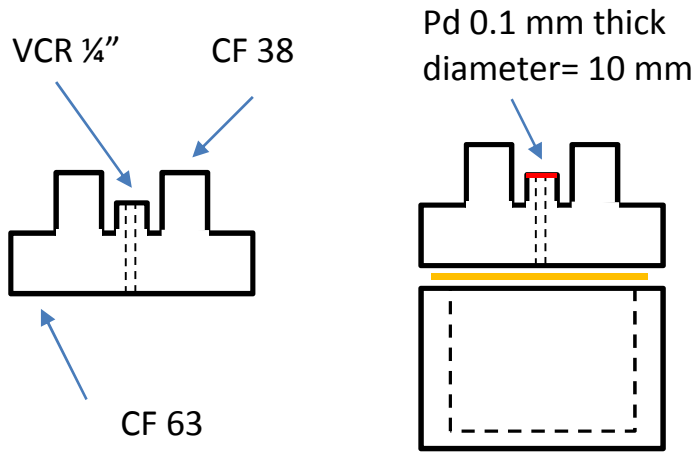

Fig. A-2. *A sketch of the lid with the membrane connection.*

A 2. Outgassing rates

A 2.1 Non-bakeable components

The valves and the pressure gauges were tested by the pressure-rise method. Each gauge was connected to a Swagelok valve and pumped down during 24 h under baking at 150-200°C. The pressure increase was measured, and from the gas volume the outgassing rate was calculated.

MKS627B pressure gauge
Pressure increase: 20 mTorr/24 h (5 cm^3) at RT.
This corresponds to an outgassing of 20x365 x5/(760x1000x24465*) = $\boldsymbol{2.0 \cdot 10^{-6}}$ ***mol/year.***
This value is a relatively high outgassing rate, which suggests that one possible source is the Inconel pressure membrane used in all MKS Baratron pressure gauges.
*24465 cm^3/mole is the molar volume of the gas at 760 Torr and 25°C.

Pfeiffer CCR 374 pressure gauge
This has ceramic membranes that cannot give off hydrogen.
Pressure increase: 0.30 mTorr/24 h (18.4 cm^3).
This corresponds to 0.30x365 x18.4/(760x1000x24465) = $\boldsymbol{1.1 \cdot 10^{-7}}$ ***mol/year***.

This gauge gives a much lower outgassing rate. Consequently, the pressure gauges for the new set-ups, Main 2 and Main 3 were exchanged to Pfeiffer CCR 374 gauges.

A 2.2 Main 2 with new pressure gauges

Baking partly at 400°C
Calculated surface area about 600 cm^2 (lid 1 side + chamber =214 x 1.5); Gas volume 350 cm^3.
Pressure increase: 3 mTorr/ 24h at RT
This corresponds to 3x365 x300/(760x1000x24465) = $\boldsymbol{2.0 \cdot 10^{-5}}$ ***mol/ year***
Outgassing / surface area is $\boldsymbol{2.2 \cdot 10^{-11}}$ ***Torr · L/s / cm²***

Baking an assembled system further at 300°C for 240 h
Pressure increase: 0.5 mTorr/24 h at RT.
This corresponds to 0.5x365 x300/(760x1000x24465) = $\boldsymbol{3.4 \cdot 10^{-6}}$ ***mol/ year***
Outgassing / surface area is $\boldsymbol{5.5 \cdot 10^{-12}}$ ***Torr · L/s · /cm²***

APPENDIX B

Measurements of hydrogen pressure, general aspects

B 1. Sieverts' law and data background.

For the equilibrium of the gas phase and the solid solution of H in Pd the following is valid:
$Pd(s) + ½xH_2(g) \rightleftharpoons PdH_x(s)$

Since $PdH_x(s)$ forms the same phase as Pd(s), only differing in composition, the hydrogen pressure depends on the composition of the solid solution. The Sieverts' law constant (K_s) is defined as the equilibrium constant, Ks for X<<1.
$K_S = \frac{P_{H_2}^{0.5}}{X}$, where X= H/Pd atomic ratio

The constant depends on the temperature, enthalpy and entropy (Ward and Dao 1999):
$K_S = e^{\left(\frac{\Delta\bar{H}_H^0}{RT} - \frac{\Delta\bar{S}_H^0}{R}\right)}$

Ward and Dao (1999) quote data published by Holleck (1970), experimentally determined in the temperature range 260 – 640°C:
$\Delta\bar{H}_H^0 = 2000\,\frac{cal}{mol}$ (The relative partial molar enthalpy of dissolution at infinite dilution)
$\Delta\bar{S}_H^0 = 11.65\,\frac{cal}{mol*K}$ (The relative partial molar entropy of dissolution at infinite dilution)
From these data Ward and Dao (1999) calculate $K_S = 351.6e^{\left(\frac{-1007}{T}\right)}$ $atm^{0.5}$

Most of the experiments in this report is at a palladium temperature of 55˚C, yielding
$K_s(55˚C) = 16.32\ atm^{0.5}$ and
$K_s(25˚C) = 12.00\ atm^{0.5}$.

By using torr as the pressure unit (conversion factor √760), the relation is rewritten as
$K_s(55˚C) = 449.903\ Torr^{0.5}$ respectively
$K_s(25˚C) = 330.85\ Torr^{0.5}$.

The constant can also be expressed with the unit $mol/cm^3\ Torr^{0.5}$.
For Pd, with density = 12 g/cm^3 and atomic mass = 106.4 g/mol,
K(55˚C)= $\mathbf{2.51 \cdot 10^{-4}}$ $mol/cm^3\ Torr^{0.5}$ and
K(25˚C)= $\mathbf{3.41 \cdot 10^{-4}}$ $mol/cm^3\ Torr^{0.5}$.

N.B. All these data were validated at higher pressures than in our experiments, typically at 1 atm. Moreover, the temperatures were higher. Both these aspects maybe influence the value of the equilibrium constant (that has been determined experimentally) to be used in other regimes of temperature and pressure.

B 2. A model for pressure correction.

The pressure corrections to the data of Main 2 and Main 3 must take care of the different volumes of the two compartments (lower and upper chamber) and the membrane, the hydrogen solubility in the membrane and must also handle the different temperatures. Since the lower chamber is heated to 50˚C for most of the experiments and at room temperature for one background measurement, while the palladium is held at 55°C, different combinations have to be considered:

I. All parts at room temperature (RT) in an empty system (background) [Main 2]
II. Lower chamber at 50˚C and the upper chamber at 25˚C. The system is empty (background) [Main 3]
III. Lower chamber at 50˚C, palladium at 55˚C and the upper chamber at 25˚C. The system is empty (background) [Complementary setup]
IV. Lower chamber at 50˚C, palladium at 55˚C and the upper chamber at 25˚C. The system is loaded (background and corrosion rates) [Main 2, Main 3]

The volumes of the system parts:
Upper chamber (above the lid): 100 cm^3
Lower chamber (reaction chamber): 250 cm^3;
Lower chamber with water, holders and Cu: 120 cm^3

Volumes for the calculations:
1. Empty system: 100 (RT) + 250 (RT or 50°C) = 350 cm^3;
2. Loaded system: 100 (RT) + 120 (RT or 50°C) = 220 cm^3

The Pd membrane:
Diameter: 10 mm; Thickness: 0.1 mm; Volume: $7.86 \cdot 10^{-3}$ cm^3
Mass: 0.094 g (density is 12 g/cm^3)

The amount of hydrogen within the Pd membrane
The amount of hydrogen in Pd:

$C_{Pd} = K(55℃) \cdot \sqrt{p} \cdot 7.86 \cdot 10^{-3}$ mol [1]

$C_{Pd}(55℃) = \sqrt{p} \cdot 1.97 \cdot 10^{-6}$ mol [2]

$C_{Pd} = K(25℃) \cdot \sqrt{p} \cdot 7.86 \cdot 10^{-3}$ mol [3]

$C_{Pd}(25℃) = \sqrt{p} \cdot 2.68 \cdot 10^{-6}$ mol [4]

However, since the gaseous form of hydrogen is a diatomic molecule,
the amount H_2 in Pd (55˚C) is $\sqrt{p} \cdot 1.00 \cdot 10^{-6}$ mol [5]
the amount H_2 in Pd (25˚C) is $\sqrt{p} \cdot 1.34 \cdot 10^{-6}$ mol [6]

The pressure yielded by the hydrogen in Pd
N.B. The standard temperature is 50˚C in the lower chamber.
The molar volume for 25˚C = 24,465 cm^3 (760 Torr)
The molar volume for 50˚C = 26,517 cm^3 (760 Torr)

The different cases (I-IV) are treated using the following nomenclature:

P_m= Measured pressure

P_{WoPd}= Calculated pressure including effect of hydrogen in palladium

Since molar amounts are being considered, the pressures can only be compared if they are multiplied with an experimental factor that involves the volume of the space and the molar volume of the gas.

Empty systems:

The volume factor for an empty system at RT (25°C) is:

$\frac{24465}{350} \cdot 760 = 53{,}124$ Torr/mol H_2 [7]

The pressure correction at 25°C is obtained from combining [6] and [7]:

$P_{WoPd} = P_m + 0.0712\sqrt{P_m}$ [8] (at 25°C)

The volume factor for an *empty* system with hydrogen at 25°C and 50°C is:

$\left(\frac{26517\left(\frac{250}{350}\right)}{350} + \frac{24465\left(\frac{100}{350}\right)}{350}\right) \cdot 760 = 56{,}307$ Torr/mol H_2 [9] (at 25°C resp. 50°C)

The pressure correction including the Pd at 55°C is obtained from combining [5] and [9]:

$P_{WoPd} = P_m + 0.0563\sqrt{P_m}$ [10] (at 25°C, 50°C resp. 55°C)

Loaded systems:

Here, part of the space is taken by the introduction of the copper samples.

The volume factor for *loaded* system with hydrogen at 25°C and 50°C is:

$\left(\frac{26517\left(\frac{120}{220}\right)}{220} + \frac{24465\left(\frac{100}{220}\right)}{220}\right) \cdot 760 = 88{,}383$ Torr/mol H_2 [11] (at 25°C resp. 50°C)

Pressure correction for a loaded system including Pd from combining [5] and [11]:

$P_{WoPd} = P_m + 0.0884\sqrt{P_m}$ [12] (at 25°C, 50°C resp. 55°C)

For comparing of outgassing between an empty and a loaded system, the volume difference between the two has to be compensated for by the ratio 1.570. That factor can be multiplied to the measured pressure and used.

The applied model has obvious limitations. It is solely based on a situation of equilibrium, and as indicated above, even the equilibrium constant (Sieverts' law) is approximated since these experiments deal with other pressures and temperatures. In the model it is not possible to introduce parameters that involve the dynamics of the system, considering hydrogen production in both the lower and the upper chamber and processes at the palladium surface. Equilibrium models can never include the time aspect, i.e. how long it takes before equilibrium is attained. These problems are most certainly reflected in the outcome of the experiments, making it difficult to extract exact values since the model is faltering.

B 3. Evaluation of the pressure measurements

In order to determine the pressure increase rate, data from both from the backgrounds and the corrosion experiments have to be included. The pressure increase is the slope of the pressure curve.

$$Rate = \frac{\partial P}{\partial t} \approx \frac{\Delta P}{\Delta t}$$

The data are evaluated in the Excel software; the slope is calculated by taking the pressure difference in an interval of approximately 83-85 h.
In order to arrive at comparable rates, Torr/h is transformed to mol/year.

The transformation formula is: $\frac{Volume\ (cm^3)\cdot 24h\cdot 360\ days}{molar\ volume\left(\frac{cm^3}{mol}\right)760}$ [13]

In this expression, the input pressure is measured in Torr and the time in hours. The molar volume at 760 Torr is 24465 cm^3/mol at 25°C and 26517 cm^3/mol at 50°C (See B 2 above).

At RT (25˚C), the factor is 0.1649.
At 50˚C, the factor is 0.1556 for an empty system and 0.09911 for a loaded system.

The rates may be plotted vs. time in order to check whether a constant rate is obtained. This kind of analysis is practised in connection with Fig. 3-4 and Figs. C-3 and C-4.

Determination of the rates for Main 3:
Data from the pressure measurements for Main 3 (Fig. 3-5) were corrected for the influence by the Pd membrane (See Appendix B 2), from which hydrogen rates were calculated (cf. Fig. 3-4 for Main 2). The result for Main 3 is given in Fig. B-1 below:

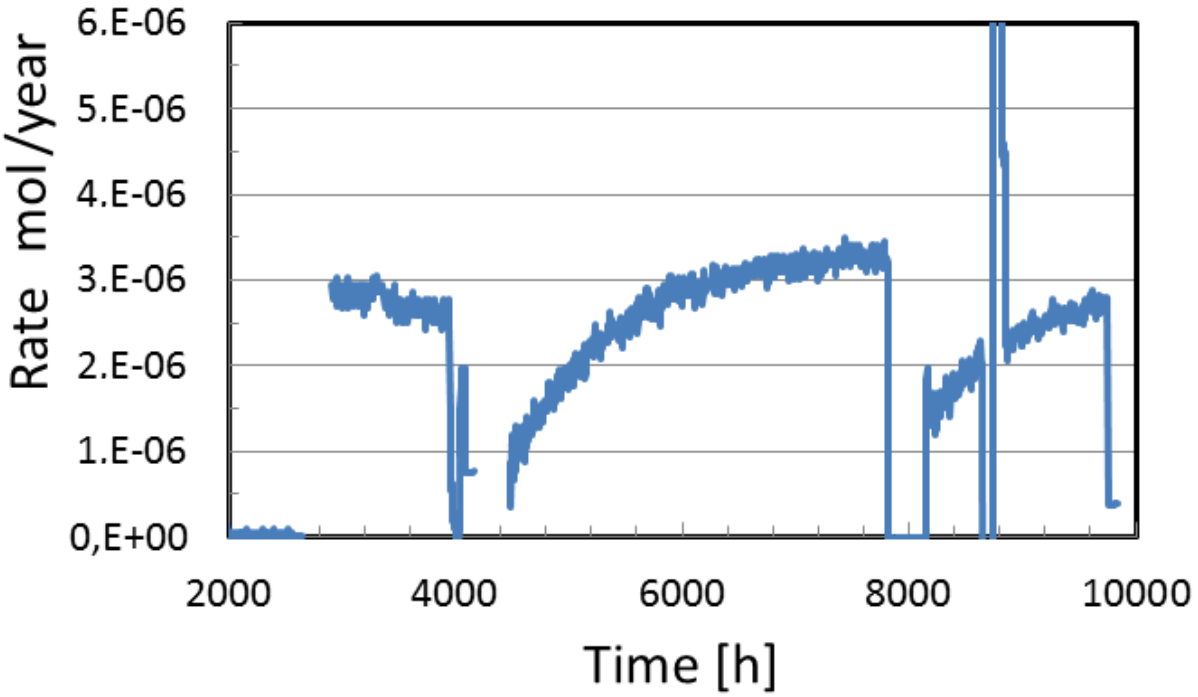

Fig. B-1. *Estimated hydrogen production rates for Main3. (Note the logging system flaw.)*

APPENDIX C

Complementary equipment

C 1. Influence by oxygen

One test with the equipment outside the glove box concerned the possibility of interference from oxygen. With this equipment pressure could be measured in both chambers, and the equalization of pressure between the chambers after any perturbation could be monitored by time.

A scheme was followed where the equipment only had a Pd membrane between the compartments but contained no water:

1. Evacuation.
2. Addition of 0.1 Torr air (0.021 Torr O_2) to the lower chamber.
3. Further addition of 0.95 Torr air.
4. Evacuation.

Monitoring was made of the equalization rate between the chambers as presented in **Fig. 3-1**.

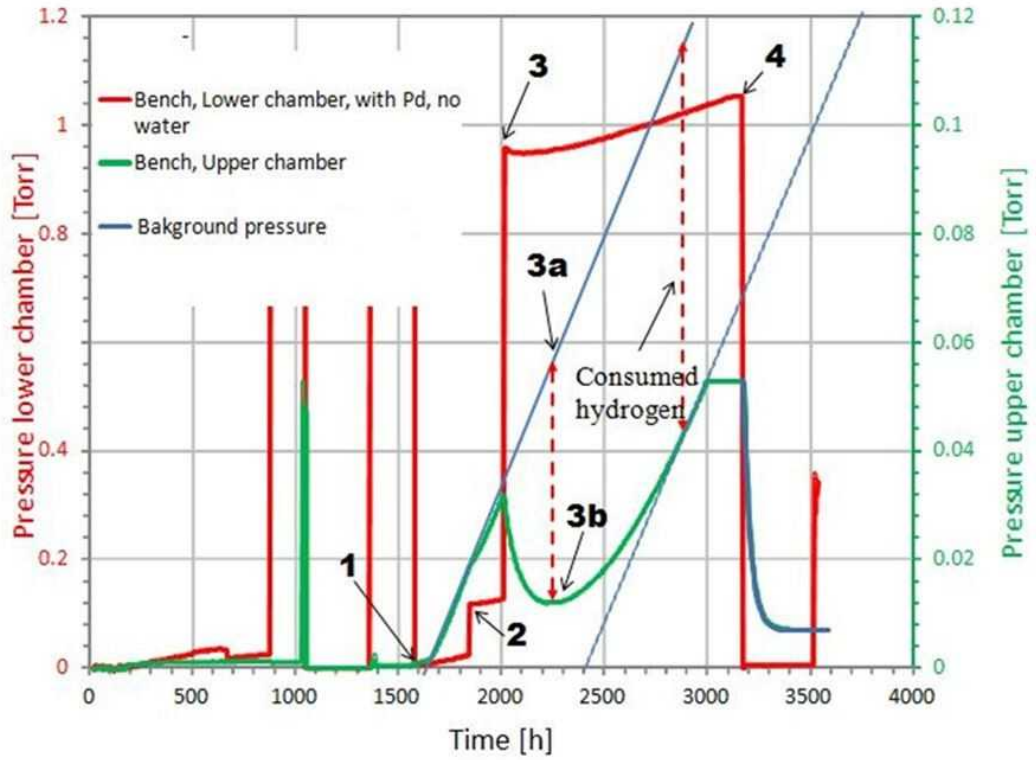

Fig. C-1. *Pressure characteristics of the experiment are described in text. Pressures may be followed in lower as well as upper chamber, these being connected through a Pd membrane for hydrogen exchange.*

The stainless steel and other parts of the system act as the only emitting sources of hydrogen. It was thus important at start to remove as much as possible of the background gas by thoroughly evacuating. The inserted numbers in the figure allude to those of the experimental scheme above, but the first step is illustrated by several evacuations during the first 1500 hours.

After about 1500 hours the evacuations were stopped. A continuous almost linear increase of pressure in the lower chamber (red line) is accompanied by the same in the upper chamber (green line – N.B. different scales). At about 1750 h, at point 2, the first addition of air is made. The rate of pressure increase in the upper chamber is altered somewhat as a result, a small lowering occurs. The pressure in the upper chamber is due to hydrogen only while there is now a gas mixture in the lower one.

At 2000 h a much larger addition of air is made (point 3) to the lower chamber, with a pronounced effect also in the upper one: Now both pressures go down and then rise again. The minimum of the hydrogen pressure in the upper chamber occurs at point 3b while point 3a denotes the pressure that would have occurred if there had not been any perturbation, assuming that the linear increase just continued. The pressures increase up to about 3200 h when (at point 4) another evacuation occurs of the lower chamber. The plateau in the green curve before that stage is an artefact created from the readings of the pressure gauge. Just after point 4 when the evacuation of the lower chamber is seen as very efficient, there is a slow response at the upper chamber, and the pressure goes to a fixed value just below 0.01 Torr.

The direct qualitative interpretation of the outcome of introducing air in the lower chamber is that the oxygen consumes hydrogen with the palladium catalysing that reaction. At the minimum in hydrogen pressure (upper chamber) the pressure has dropped from the unperturbed expected pressure of 0.054 Torr (point 3a) to 0.012 Torr (point 3b). After the minimum, there is again an increase in pressure with a rate that is approaching that of the unperturbed system (slope of tangent at 3000 h), a value of ~0.12 Torr/1500 h. The displacement of the tangent in comparison with the extrapolated rate before the perturbation is a measure of the amount of hydrogen taking part in the reaction with oxygen. This corresponds to a pressure difference of 0.070 Torr (e.g. at arrows at ~2900 h in the figure).

The amount of consumed hydrogen relates to 0.070 Torr in 350 cm^3 (= 24.5 Torr·cm^3). The amount of added oxygen from the air was 0.95 Torr x 0.21 x 250 cm^3 = 49.9 Torr·cm^3. The found molar ratio of H_2 and O_2 is then roughly 1:2.

The important conclusion from this experiment series is that the palladium membrane seems to take an active part as a catalyst so that water forms. However, this experiment cannot elucidate the role that the membrane itself takes as it dissolves hydrogen (that would otherwise have reacted further with oxygen). This effect of forming a solid solution, PdH_x, affects the determination of the background.

C 2. Determination of background outgassing rates

The background of the complementary setup was investigated through a series of measurements with intermittent pumping. The pressure curves are shown in **Fig. C-2**, the left part of which constitutes **Fig. C-1**. The same nomenclature is used, *i.e.* green curves and scale belong to the upper chamber, and red ones to the lower chamber.

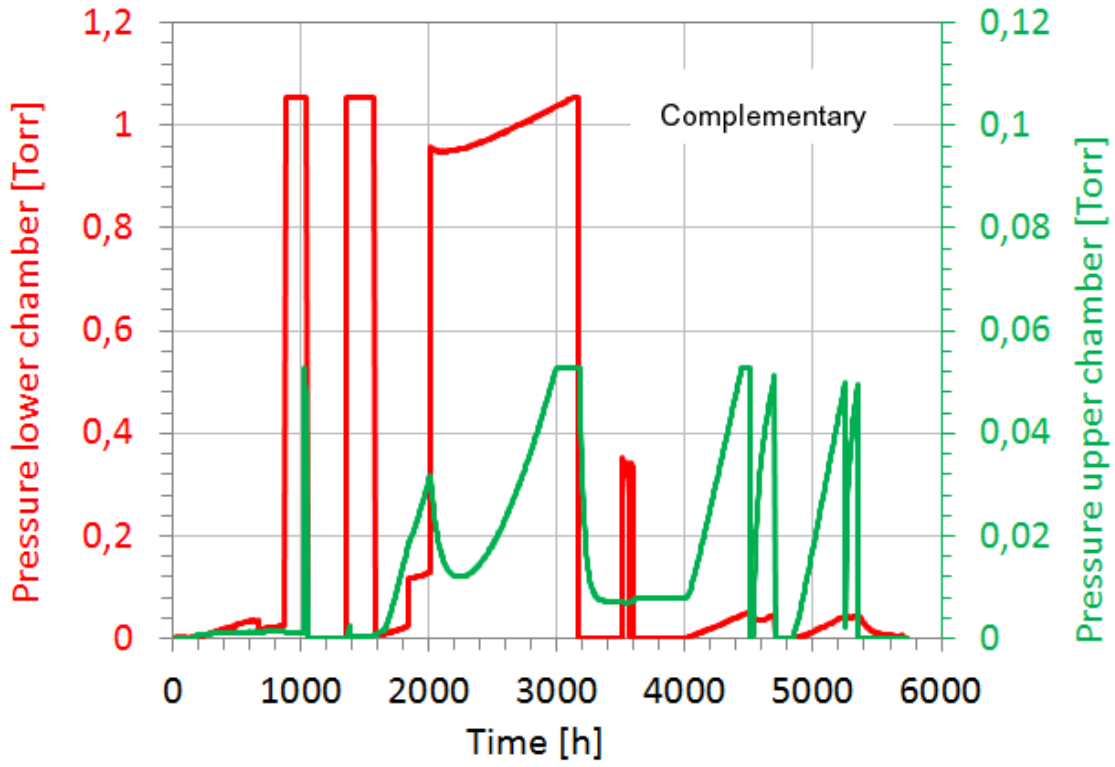

Fig. C-2. *Supplemented data of Fig. C-1. The background measured after 4000 hrs are only due to the outgassing from the stainless steel.*

The outgassing rates could be calculated from the pressure curves using the model described previously in Appendix B. Specifically, the model III of section B 2 (equation [10] there) is to be used. The connection between the pressures is expressed by

$$P_{WoPd} = P_m + 0.0563\sqrt{P_m}\ .$$

The transformation to molar amounts of hydrogen gas (H_2) from the relation $\frac{P_m \cdot 350 \cdot 24 \cdot 365}{26517 \cdot 760}$ yields a production of P_{WoPd} ·0.1552 mol/year (pressures in Torr).

The background pressures were measured in the time period 4000-5400 hrs but also before the inlet of air (See Table C-1). The transformation into rates is displayed in Figs. C-3 and C-4. “Stable” and “unstable” figuratively describe whether a fair value could be obtained or not.

Table C-1. *Estimations of outgassing rates (mol/year) from measurements and modelling*

Time period	Upper chamber	Comment	Lower chamber	Comment
1800-1900	$1.9 \cdot 10^{-5}$	Unstable	$1.7 \cdot 10^{-5}$	Unstable
4000-4700	$2.0 \cdot 10^{-5}$	Stable	$1.9 \cdot 10^{-5}$	Stable
4900-5400	$2.3 \cdot 10^{-5}$	Unstable	$2.2 \cdot 10^{-5}$	Stable

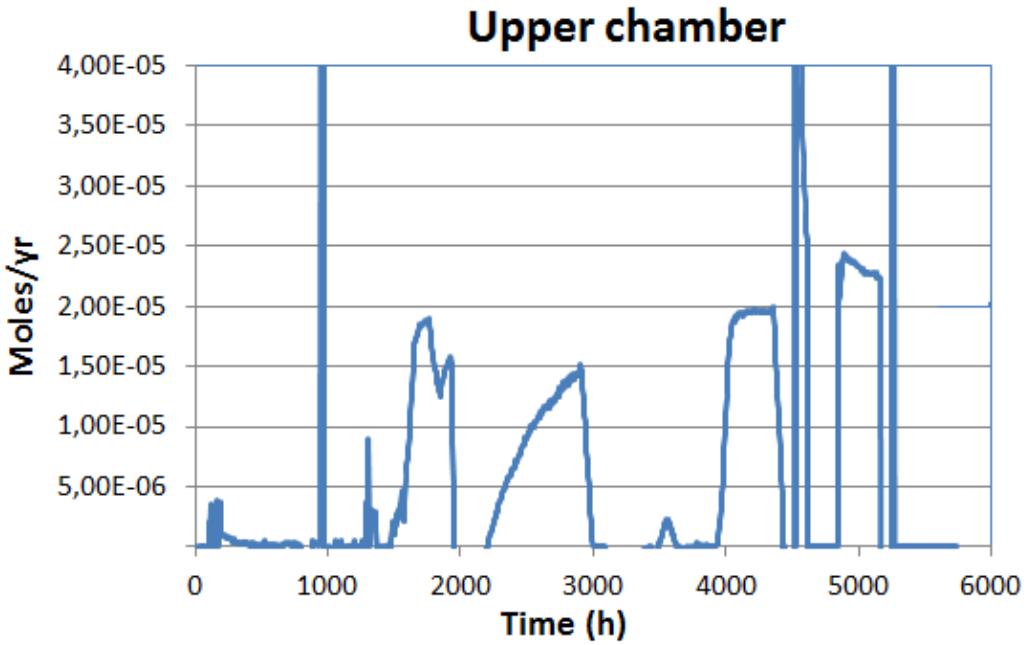

Fig. C-3. *Calculated outgassing rates from data of the upper chamber (green curves of Fig. C-2) using the relations given in text.*

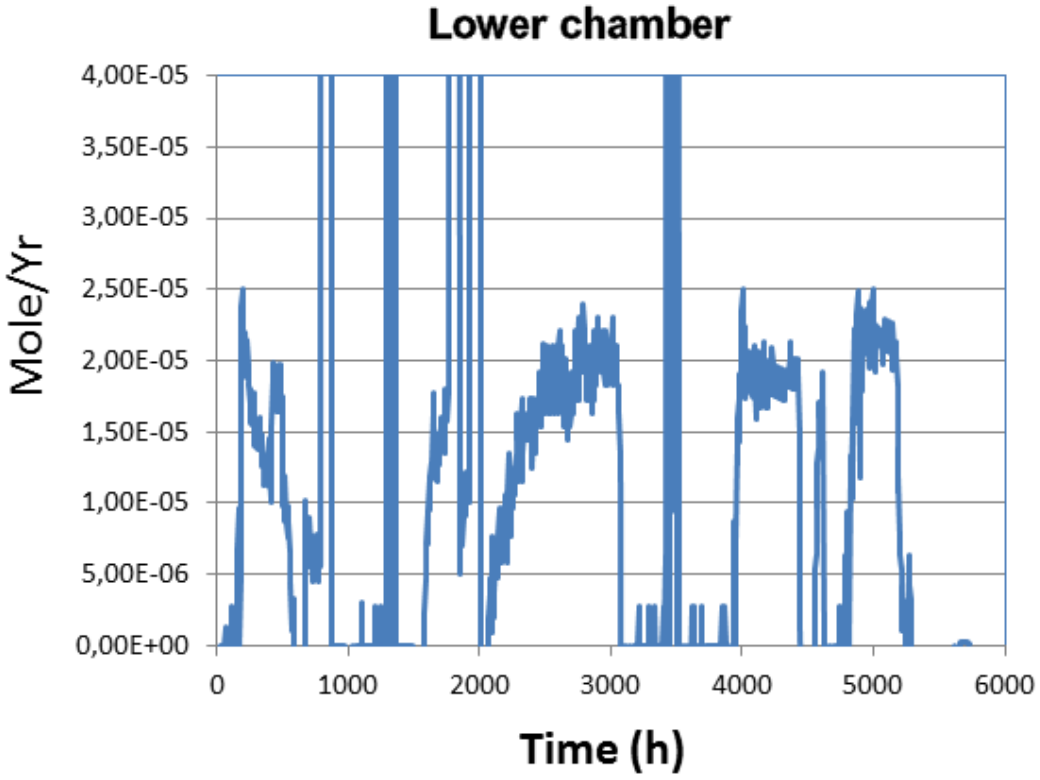

Fig. C-4. *Calculated outgassing rates from data of the lower chamber (red curves of Fig. C-2) using the relations given in text.*

C 3. Pressure equilibration between the chambers

C 3.1 Addition of a H_2/N_2 mixture

In order to investigate the response time between the lower reaction chamber (of volume 250 cm^3) and the pressure gauges in the upper chamber (100 cm^3), an H_2/N_2 mixture was added to the lower chamber. The question raised was whether nitrogen in excess (that is present because of the glove-box environment) would hamper the exchange to any considerable extent. A gas mixture with very low hydrogen content was chosen, but the situation is not directly comparable with that in Main 1-3, in the sense that the pressure difference between the two chambers is roughly ten times higher than in any of the experiments concerning copper corrosion.

1. Both chambers were pumped down during about 30 h
2. The lower chamber (250 cm^3) was filled to 752 Torr by a H_2/N_2 mixture (1000 ppm H_2)
3. The pressure increase in the upper chamber (100 cm^3) was measured

The pressure without any Pd in the total system volume (350 cm^3) would be
$752 \times 1.00 \cdot 10^{-3} \times 250 cm^3 / 350 cm^3 = 0.537$ Torr
P_m= the expected (real/measured) pressure would be = 0.496 Torr (See Appendix C 3.2 , quoting B 2, eq. [10]).

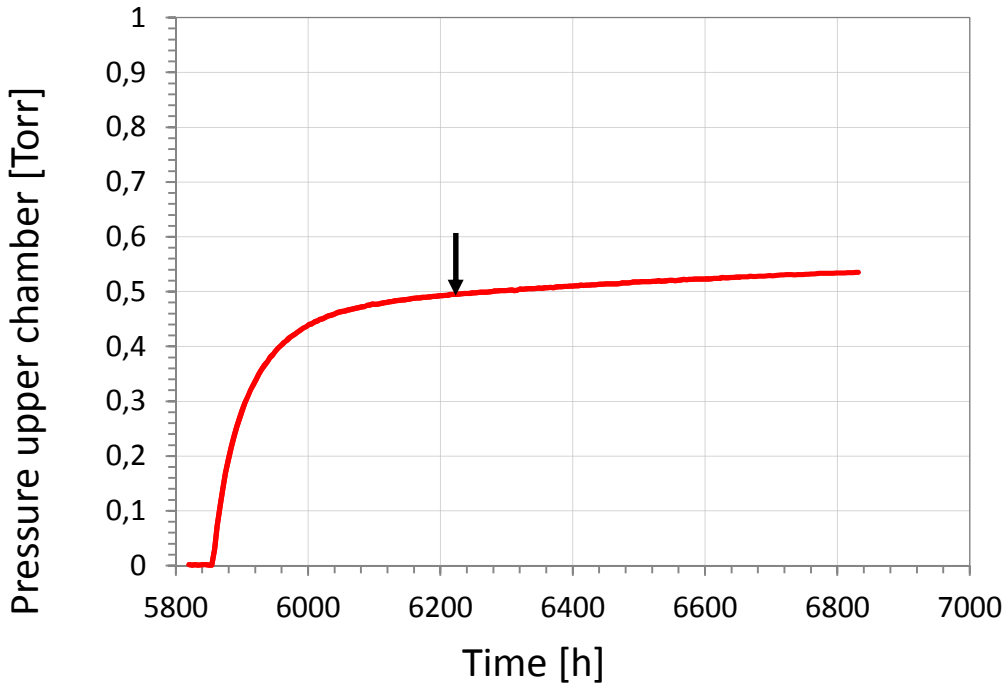

Fig. C-5. *Pressure equilibration after addition of gas mixture. The expected pressure (see text) of 0.496 Torr is marked with an arrow.*

C 3.2 Calculation of the pressure increase with the Pd foil

The relation $P_{WoPd}=P_m + K_{exp} \sqrt{P_m}$ (See 3.2.1), where

P_m = The measured pressure
P_{WoPd}= The pressure without Pd
K_{exp} = Experimental constant, including K_s and volume factor

may be rewritten as on a quadratic form as

$$P_m^2 - (2P_{WoPd} + K_{exp}^2)P_m + P_{WoPd}^2 = 0$$

Its solution is $P_m = ½K_{exp}^2 + P_{WoPd} - ½K_{exp}\sqrt{K_{exp}^2 + 4P_{WoPd}}$

K_{exp}= 0.0563 for a system temperature of 50˚C, Pd temperature of 55˚C (Appendix B 2, [10])

In this case one may arrive at the approximation $P_m = P_{WoPd} - K_{exp}\sqrt{P_{WoPd}}$

C 3.3 Relaxation time

By plotting the pressure increase rate, the relaxation time can be determined.
In order to arrive at comparable rates, Torr/h is transformed to mol/year.

The transformation formula is: $\frac{Volume\ (cm^3)\cdot 24h\cdot 360\ days}{molar\ volume\left(\frac{cm^3}{mol}\right)760}$ (Appendix B 3, [13])

In this expression, the input pressure is measured in Torr and the time in hours. The molar volume at 760 Torr is 26,,517 cm^3/mol at 50°C (From Appendix B 2).

When the rate decreases to the value of the outgassing ($2\cdot 10^{-5}$ mol/year; *cf.* Table C-1), the relaxation is complete. From Fig. C-6, this rate is obtained at 6,175 h or 355 h after the addition of the hydrogen/nitrogen mixture.

From this behaviour, the conclusions are that the relaxation time is several hundred hours for attaining equilibrium between the two chambers. The important thing is that the nitrogen is not preventing an exchange of hydrogen between the chambers and that full equilibrium is obtained. In this respect this experiment has bearing on the experimental setups Main1-3 where the start means a nitrogen atmosphere from the glove box.

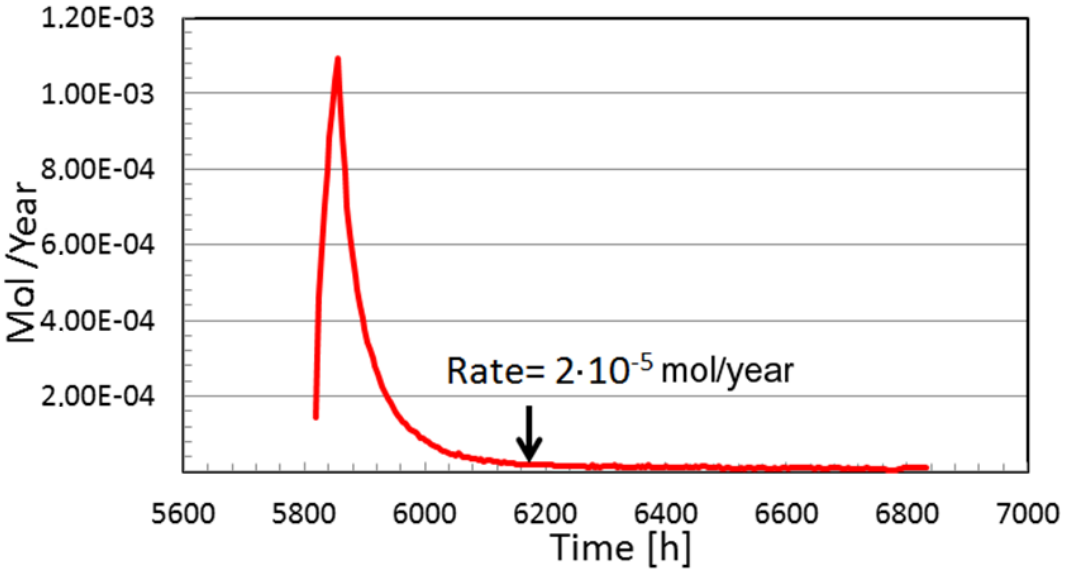

Fig. C-6. *Rate evolution from Fig. C-5.*

APPENDIX D

Details of ICP-MS analyses

The results presented in **Fig. 3-16** are here given in numerical form:

Element\ months		0	1	3	6	15	29
Ag	(µg/l)	0.07	0.04	0.03	0.04	0.04	0.03
Al	(µg/l)	32	12	73	222	239	275
As	(µg/l)	0.06	0.04	0.03	0.04	0.04	0.04
B	(µg/l)	*172	112	341	672	854	1734
Ba	(µg/l)	0.26	0.39	0.15	0.51	0.35	0.20
Br	(µg/l)	1.00	0.79	0.85	1.04	1.61	1.43
Ca	(µg/l)	94	40	103	223	197	241
Cd	(µg/l)	0.01	0.11	0.00	0.00	0.01	0.10
Cl	(µg/l)	167	143	142	146	115	44
Cr	(µg/l)	0.53	0.44	0.46	0.55	0.66	0.31
Cu	(µg/l)	0.90	6.29	5.53	8.33	4.95	19.0
Fe	(µg/l)	0.53	1.55	0.45	1.37	1.91	1.67
Ga	(µg/l)	0.05	0.74	0.57	0.58	0.65	0.39
Ge	(µg/l)	0.01	0.29	0.57	0.06	0.08	0.09
Hf	(µg/l)	0.00	0.00	0.00	0.01	0.26	0.20
I	(µg/l)	1.86	1.61	0.95	1.27	1.55	0.52
K	(µg/l)	300	157	431	854	1104	1344
Li	(µg/l)	1.03	0.72	1.29	1.67	1.41	1.38
Mg	(µg/l)	5.09	4.84	5.31	8.53	7.27	7.56
Mn	(µg/l)	0.03	0.04	0.02	0.04	0.04	0.06
Mo	(µg/l)	0.02	0.02	0.04	0.07	0.08	0.12
Na	(µg/l)	273	211	446	811	953	1057
P	(µg/l)	3.21	27.11	17.79	13.81	11.68	23.32
Pb	(µg/l)	0.02	0.13	0.01	0.04	0.13	2.58
Rb	(µg/l)	0.07	0.04	0.11	0.23	0.25	0.28
Sb	(µg/l)	4.26	3.33	6.62	5.68	15.85	22.22
Sc	(µg/l)	0.60	0.15	0.76	0.99	1.30	1.24
Se	(µg/l)	0.17	0.16	0.13	0.13	0.15	0.17
Si	(µg/l)	4883	1187	6939	9282	12679	12151
Sr	(µg/l)	0.06	0.01	0.05	0.12	0.08	0.07
Ti	(µg/l)	0.41	0.28	0.52	0.69	1.27	1.33
Tl	(µg/l)	0.03	0.03	0.04	0.04	0.04	0.04
V	(µg/l)	0.02	0.01	0.02	0.02	0.03	0.05
W	(µg/l)	0.02	0.03	0.03	0.03	0.08	0.08
Y	(µg/l)	0.00	0.22	0.02	0.02	0.03	0.03
Zn	(µg/l)	5.62	7.11	7.76	8.00	7.67	8.62
Zr	(µg/l)	0.01	0.03	0.06	0.42	7.95	6.89

*The most abundant elements (from the glass) are high-lighted in yellow

APPENDIX E

Hydrogen analyses

E 1. Hydrogen desorption experiments

E 1.1 Testing of procedure

Experiments were also performed on other copper material for testing the purification procedure concerning hydrogen desorption, namely the efficiency to remove dissolved hydrogen as a function of temperature. Pristine copper samples from Goodfellow (99.95%) and from Alpha Aesar (99.9999%) were heated up to 600°C at a rate of 1°C/min. At this heating rate, there is no difference between sample and furnace temperature. The outcome of this treatment, from the hydrogen signal in a mass spectrometer (QMS), is illustrated in **Fig. E-1**. As may be noted from this figure, the base pressures of the system were different. Hydrogen is effectively desorbed within a temperature range of 350 – 500°C with a maximum evolution at 400°C for moderate heating rates. This temperature was chosen *ad hoc* for the final purification step of the ultrapure copper used in this investigation as well as in Boman et al. (2014), in that case after electropolishing and hydrogen reduction. The outcome of heat treatment at that temperature was followed by QMS as illustrated in **Fig. 3-13.** The peak in **Fig. E-1** occurring at about 300°C, irrespective of purity grade, may emanate from hydrogen bound near the surface.

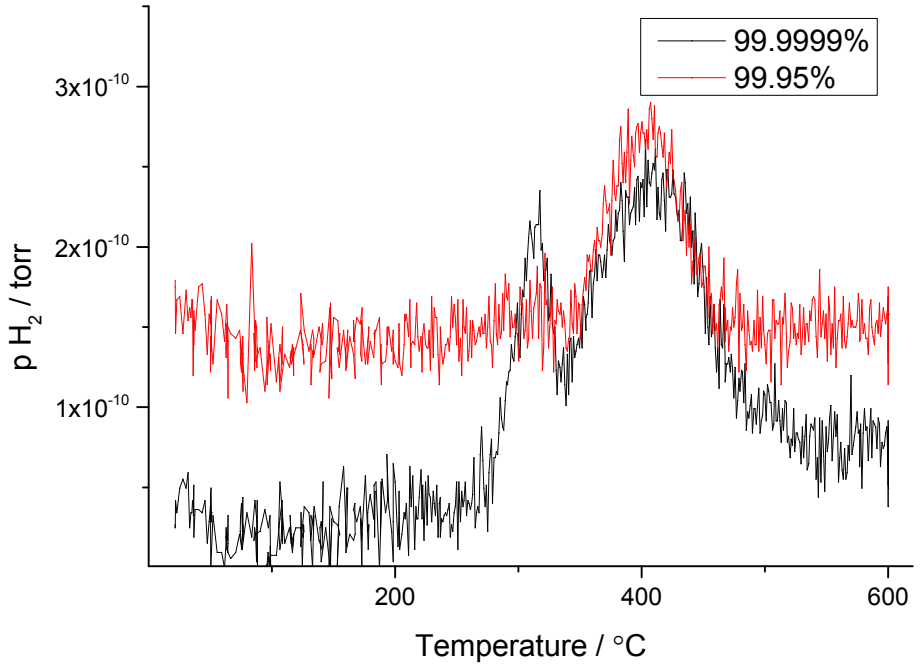

Fig. E-1. *The hydrogen pressure as a function of temperature from copper samples of different purities. The mass of the 99.9999% pure sample (black curve) is 6 times larger than that of the less pure copper (red).*

E 1.2 Studies of samples sent for fusion analysis (LECO)

The following figures illustrate the desorption of hydrogen and other selected species from copper samples that were later sent for fusion analysis of the hydrogen content to Degerfors Laboratorium AB (Analysis certificates under Appendix E 3), the results of which are quoted. The sample masses were 5-6 g and the surfaces were not polished before the analyses.

The various species that were recorded (QMS) are colour coded. For each sample there are pairs of figures, where the right-hand figure shows the same data as the one at the left, only that the contribution by water (blue) has been removed and the data are rescaled so that the contributions of the rest appear larger in size. Hydrogen is marked by deep red, and the area under the red curve correlates to the amount of hydrogen in the sample.

Sample Cu1, "as received"

The hydrogen content before heating to 600°C is 0.7 ppm and after 0.06 ppm.

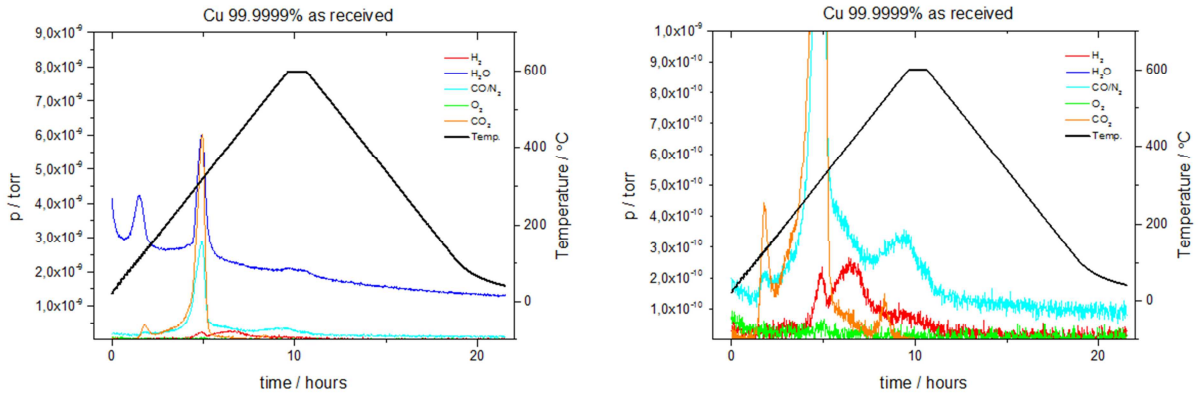

a. **b.**

Fig. E-2 a-b. *Measured pressures of the gas species vs. time/temperature obtained on heating/cooling for Cu 1. The signal marked CO, N2 belongs to CO.*

Sample Cu2, after electropolishing

Hydrogen content after electropolishing is 0.16 ppm. As shown, most of the hydrogen is removed from the surface layer during the electropolishing process.

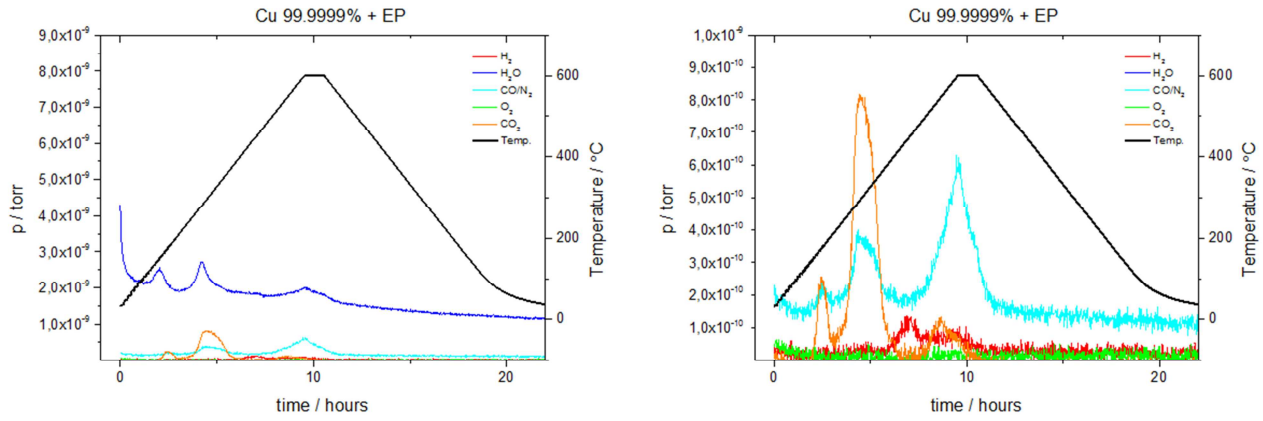

Fig. E-3 a-b. *Measured pressures of the gas species vs. time/temperature obtained on heating/cooling for Cu 2.*

Sample Cu4, after electropolishing and hydrogen treatment
The hydrogen content remained low (0.03 ppm) after this treatment"

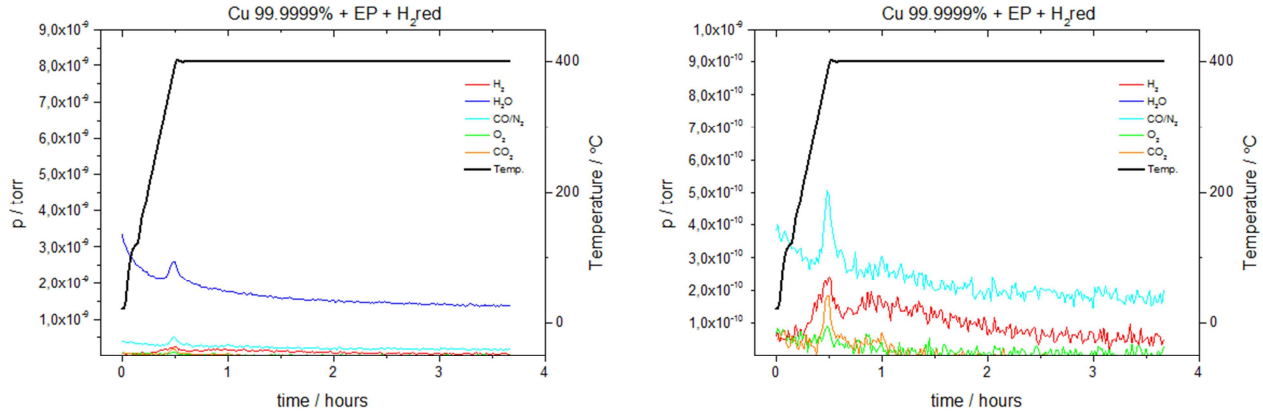

Fig. E-4 a-b. *Measured pressures of the gas species vs. time/temperature obtained on heating/cooling for Cu 4*

Because of different molecular properties, the areas under the curves cannot be used for a direct comparison between different species. None of the samples were kept under inert conditions prior to the analysis. Hence, the surface is contaminated to a certain degree. Water first disappears at about 100°C which may be an effect of chemisorption or the decomposition of superficial copper(II) hydroxide. Harder bound water is removed at about 300°C together with CO_2, possibly from a hydroxide carbonate of copper. A detailed analysis lies outside the scope of this study.

E 2. Fusion analysis, previous trials

As alluded to in section 3.4.1, samples were earlier sent for fusion analysis where normal procedure was followed, i.e. the specimens were polished before analysis. As seen from Table E-1, there is a large spread in the values obtained. This was interpreted as an effect either of inhomogeneity or of small sample size. All analysis methods have their optimum, and in a second attempt larger sizes were used, and the surface was left intact. As seen in section 3.4.1 these instructions rendered significantly smaller values and better precision.

The differences in procedure and sample size are probable reasons for the still higher contents obtained from the analyses reported in Boman et al. (2014).

Values from the new attempt (no polishing, larger size – 5-6 grams) are found in section 3.4.1 and the corresponding analysis certificates (values being an average from two measurements) in Appendix E-3.

Table E-1. *Hydrogen content as determined by the LECO method after surface polishing*

Copper sample	As received	Electropolished	15 months' sample
Hydrogen content (ppm)	0.1 – 1.9	0.2 – 1.2	0.3

E 3. Fusion analysis certificates from new trials

D-LAB
DEGERFORS LABORATORIUM AB

Provningsresultat / Test Results:

Ordernr / Ordemo: DL-33872

Beställare / Client	Referens / Reference
Uppsala Universitet	**Pedro Berastegui**
Adress / Address: Box 538, 751 21 UPPSALA	

Er beställning / Your order No	Ankomstdag / Sample Registration Date	Utskriftsdatum / Date of issue	DL ID
139EVL Pedro Berastegui	2015-01-19	2015-01-19	533132

Provbeteckning / Sample identity: Cu1 As received (AR)

Noteringar / Notes:

Resultat/Results

H	0.7 ppm

Note: Not responsible for electronically transferred reports due to changes of data during transmission. Please contact us in doubtful cases.

DEGERFORS LABORATORIUM

Ingvar Bernhardsson
Kvalitetschef

Degerfors Laboratorium AB
Box 54
SE-693 21 DEGERFORS
SWEDEN

Phone +46 586 47406
Fax: +46 586 47005

Web: www.degerforslab.se
Email: sebackman@degerforslab.se
VAT no.: SE 556609044401

Bankgiro: 5735-6784
Bank: Foreningssparbanken, Degerfors
IBAN: SE8480000815629833744494
BIC/SWIFT: SWEDSESS

D-LAB
DEGERFORS LABORATORIUM AB

Provningsresultat / Test Results:

Ordernr / Ordernr
DL-33872

Beställare / Client	Referens / Reference
Uppsala Universitet	**Pedro Berastegui**
Adress / Address	
Box 538, 751 21 UPPSALA	

Er beställning / Your order No	Ankomstdag / Sample Registration Date	Utskriftsdatum / Date of issue	DL ID
139EVL Pedro Berastegui	2015-01-19	2015-01-19	533133

Provbeteckning / Sample identity
Cu2 AR + Elektropolerat I H3PO4

Noteringar / Notes

Resultat/Results

H	0.16 ppm

Note: Not responsible for electronically transferred reports due to changes of data during transmission. Please contact us in doubtful cases.

DEGERFORS LABORATORIUM

Ingvar Bernhardsson
Kvalitetschef

Degerfors Laboratorium AB
Box 54
SE-693 21 DEGERFORS
SWEDEN

Phone +46 586 47406
Fax: +46 586 47005

Web: www.degerforslab.se
Email: sebackman@degerforslab.se
VAT no.: SE 556609044401

Bankgiro: 5735-6784
Bank: Foreningssparbanken, Degerfors
IBAN: SE8480000815629833744494
BIC/SWIFT: SWEDSESS

D-LAB
DEGERFORS LABORATORIUM AB

Provningsresultat / Test Results:

Ordernr / Ordernr
DL-33872

Beställare / Client	Referens / Reference
Uppsala Universitet	**Pedro Berastegui**
Adress / Address	
Box 538, 751 21 UPPSALA	

Er beställning / Your order No	Ankomstdag / Sample Registration Date	Utskriftsdatum / Date of issue	DL ID
139EVL Pedro Berastegui	2015-01-19	2015-01-19	533134

Provbeteckning / Sample identity
Cu3 AR + EP + Reducerat I H2 I 300C

Noteringar / Notes

Resultat/Results

H	0.03 ppm

Note: Not responsible for electronically transferred reports due to changes of data during transmission. Please contact us in doubtful cases.

DEGERFORS LABORATORIUM

Ingvar Bernhardsson
Kvalitetschef

Degerfors Laboratorium AB
Box 54
SE-693 21 DEGERFORS
SWEDEN

Phone +46 586 47406
Fax: +46 586 47005

Web: www.degerforslab.se
Email: sebackman@degerforslab.se
VAT no.: SE 556609044401

Bankgiro: 5735-6784
Bank: Foreningssparbanken, Degerfors
IBAN: SE8480000815629833744494
BIC/SWIFT: SWEDSESS

D-LAB
DEGERFORS LABORATORIUM AB

Provningsresultat / Test Results:

Ordernr / Ordernr: DL-33872

Beställare / Client	Referens / Reference
Uppsala Universitet	**Pedro Berastegui**

Adress / Address: Box 538, 751 21 UPPSALA

Er beställning / Your order No	Ankomstdag / Sample Registration Date	Utskriftsdatum / Date of issue	DL ID
139EVL Pedro Berastegui	2015-01-19	2015-01-19	533135

Provbeteckning / Sample identity: Cu4 AR + EP + RH2 Värmebehandlat 400C

Noteringar / Notes:

Resultat/Results

H	0.03 ppm

Note: Not responsible for electronically transferred reports due to changes of data during transmission. Please contact us in doubtful cases.

DEGERFORS LABORATORIUM

Ingvar Bernhardsson
Kvalitetschef

Degerfors Laboratorium AB
Box 54
SE-693 21 DEGERFORS
SWEDEN

Phone +46 586 47406
Fax: +46 586 47005

Web: www.degerforslab.se
Email: sebackman@degerforslab.se
VAT no.: SE 556609044401

Bankgiro: 5735-6784
Bank: Foreningssparbanken, Degerfors
IBAN: SE8480000815629833744494
BIC/SWIFT: SWEDSESS

D-LAB
DEGERFORS LABORATORIUM AB

Provningsresultat / Test Results:

Ordernr / Ordernr
DL-33872

Beställare / Client	Referens / Reference
Uppsala Universitet	**Pedro Berastegui**
Adress / Address	
Box 538, 751 21 UPPSALA	

Er beställning / Your order No	Ankomstdag / Sample Registration Date	Utskriftsdatum / Date of issue	DL ID
139EVL Pedro Berastegui	2015-01-19	2015-01-19	533136
Provbeteckning / Sample identity			
Cu5 AR+Värmebehandlat I 600C			
Noteringar / Notes			

Resultat/Results

H	0.06 ppm

Note: Not responsible for electronically transferred reports due to changes of data during transmission. Please contact us in doubtful cases.

DEGERFORS LABORATORIUM

Ingvar Bernhardsson
Kvalitetschef

Degerfors Laboratorium AB
Box 54
SE-693 21 DEGERFORS
SWEDEN

Phone +46 586 47406
Fax: +46 586 47005

Web: www.degerforslab.se
Email: sebackman@degerforslab.se
VAT no.: SE 556609044401

Bankgiro: 5735-6784
Bank: Foreningssparbanken, Degerfors
IBAN: SE8480000815629833744494
BIC/SWIFT: SWEDSESS

D-LAB
DEGERFORS LABORATORIUM AB

Provningsresultat / Test Results:

Ordernr / Ordernr
DL-33872

Beställare / Client	Referens / Reference
Uppsala Universitet	**Pedro Berastegui**

Adress / Address
Box 538, 751 21 UPPSALA

Er beställning / Your order No	Ankomstdag / Sample Registration Date	Utskriftsdatum / Date of issue	DL ID
139EVL Pedro Berastegui	2015-01-19	2015-01-19	533137

Provbeteckning / Sample identity
28Mån prov

Noteringar / Notes

Resultat/Results

H	0.09 ppm

Note: Not responsible for electronically transferred reports due to changes of data during transmission. Please contact us in doubtful cases.

DEGERFORS LABORATORIUM

Ingvar Bernhardsson
Kvalitetschef

Degerfors Laboratorium AB
Box 54
SE-693 21 DEGERFORS
SWEDEN

Phone +46 586 47406
Fax: +46 586 47005

Web: www.degerforslab.se
Email: sebackman@degerforslab.se
VAT no.: SE 556609044401

Bankgiro: 5735-6784
Bank: Foreningssparbanken, Degerfors
IBAN: SE8480000815629833744494
BIC/SWIFT: SWEDSESS

APPENDIX F

Pressure logging of the Main 1 setup

F 1. Pressure evolution at 50°C

In **Fig. F-1** the whole logging of the Main 1 setup is given (together with two reference systems). Part of this, up to 6700 hrs, was included in Boman et al. (2014, Section 5.1) and analysed there. Recent experiments include changing of temperature.

F 2. The influence of temperature on the steady-state pressure

In order to clarify the different regimes of **Fig. F-1**, the following tableau is given for consultation. The temperature of the lower chamber was in the beginning set to 50°C, but the Pd membrane was kept at 55°C. The upper chamber held approximately 25°C. Only after 18000 hrs was the temperature changed from 50°C while the membrane temperature was set 5 degrees higher:

1. 1500 h: Steady state pressure (0.065 Torr)
2. 4000 h: Pumping and QMS analyses.
3. 9000 h: Pumping
4. 10.000 h: Ditto
5. 11.700 h: Ditto
6. 18.000 h: Temperature was set to 30˚C
7. 21.000 h: Temperature was set to 40˚C
8. 23.800 h: Temperature was set to 70˚C

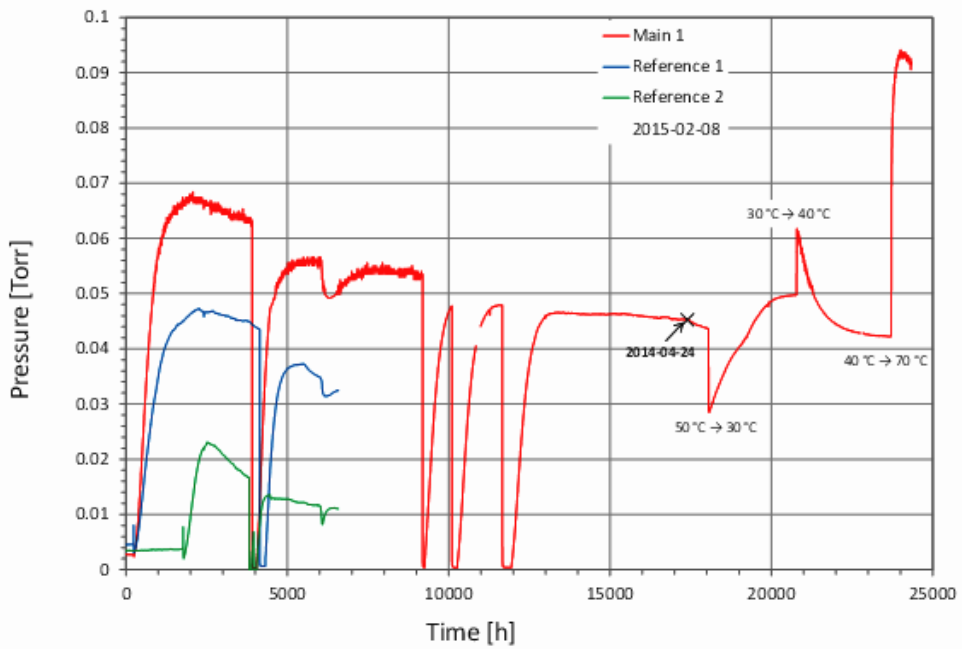

Fig F-1. *Gas pressure as a function of time (and temperature) in the upper compartment of Main 1 (and up to 6700 hrs also in reference systems).*

The temperature change-pressure response can be divided into three different steps:

1. Palladium releases or takes up hydrogen from the gas phase. This is a fast reaction.
2. Pressure changes to create a steady state between the hydrogen outgassing/production and the outleaking through the Pd membrane (Old system). This is a relatively slow process that takes up to 3000 h
3. Steady-state pressure

Table F-1. *Analysis of the data in Fig. F-1.*

Temperature System	**Temperature Palladium**	**Initial pressure Fast change Torr**	**Steady-state Torr**
50˚C	55˚C	-	0.065-0.045
30˚C	35˚C	0.028	0.048
40˚C	45˚C	0.063	0.043
70˚C	75˚C	0.085-0.093	0.093 (Jan. 2015) On-going exp.

The time to obtain a steady-state (about 3000 h) for 30˚C and 40˚C can be compared with the time for steady-state after pumping the system, about 1000 - 1500 h.

The measurements illustrate two important facts (**Fig. F-1, Table F-1**). First of all, the attaining of a steady-state condition after a change takes considerable time. Secondly, the effect of hydrogen dissolution in the Pd membrane is evident.

Because of the competition between reactions that carry different temperature dependence (different activation energies), there is no evident trend to read from the temperatures and the steady-state pressure eventually obtained. The situation is too complex to make modelling feasible without a more thorough analysis.